ISSN 1991-1696

# Africa Research Journal

Research Journal of the South African Institute of Electrical Engineers

Incorporating the SAIEE Transactions

SAIEE AFRICA RESEARCH JOURNAL Vol 100 No.2 pp 32-58

www.saiee.org.za

June 2009
Volume 100 No. 2

# SAIEE AFRICA RESEARCH JOURNAL

**(SAIEE FOUNDED JUNE 1909 INCORPORATED DECEMBER 1909)**
**AN OFFICIAL JOURNAL OF THE INSTITUTE**
**ISSN 1991-1696**

**President**
Mr du Toit Grobler
**Vice-Presidents**
Mr Andries Tshabalala
Mr Mike Cary

**Immediate Past President**
Mr Ian McKechnie
**Deputy President**
Mr Angus Hay
**Honorary Treasurer**
Mr Les James

**Secretary and Head Office**
Ms Gerda Geyer
South African Institute for Electrical Engineers (SAIEE)
PO Box 751253, Gardenview, 2047, South Africa
Tel: (27-11) 487-3003
Fax: (27-11) 487-3002
E-mail: geyerg@saiee.org.za

**Editorial Board**
Chairperson Prof IK Craig

ARJ Editor-in-Chief Prof BM Lacquet

## EDITORS AND REVIEWERS

**EDITOR-IN-CHIEF**
**Prof. B.M. Lacquet**, Faculty of Engineering and the Built Environment, University of Witwatersrand, Johannesburg, South Africa
beatrys.lacquet@wits.ac.za

**MANAGING EDITOR**
**Dr S. Sinha**, Dept. of Electrical, Electronic & Computer Engineering, University of Pretoria, Pretoria, South Africa ssinha@ieee.org

**SPECIALIST EDITORS**
**Communications, Signal Processing:**
**Prof. L.P. Linde,** Dept. of Electrical, Electronic & Computer Engineering, University of Pretoria, Pretoria, South Africa
**Prof. S. Maharaj**, Dept. of Electrical, Electronic & Computer Engineering, University of Pretoria, Pretoria, South Africa
**Dr O Holland,** Centre for Telecommunications Research, London, United Kingdom
**Prof. F. Takawira,** School of Electrical, Electronic and Computer Engineering, University of KwaZulu-Natal, Durban, South Africa
**Computer, Information Systems and Software Engineering:**
**Prof. A. van der Merwe,** Meraka Institute, Pretoria, South Africa
**Prof. E. Barnard,** Meraka Institute, Pretoria, South Africa
**Prof. B. Dwolatzky**, Joburg Centre for Software Engineering, University of the Witwatersrand, Johannesburg, South Africa
**Control and Automation:**
**Dr B. Yuksel,** University of Tokyo, Japan
**Electromagnetics and Antennas:**
**Prof. J.H. Cloete**, Dept. of Electrical and Electronic Engineering, University of Stellenbosch, South Africa 5 Electron Devices and Circuits
**Prof. T.J.O. Afullo,** School of Electrical, Electronic and Computer Engineering, University of KwaZulu-Natal, Durban, South Africa
**Dr R. Geschke,** Dept. of Electrical and Electronic Engineering, University of Stellenbosch, South Africa
**Electron Devices and Circuits:**
**Prof. M. du Plessis**, Dept. of Electrical, Electronic & Computer Engineering, Pretoria, University of Pretoria, South Africa
**Energy and Power Systems:**
**Prof. M. Delimar,** Faculty of Electrical Engineering and Computing, University of Zagreb, Zagreb, Croatia
**Engineering and Technology Management:**
**Prof. J-H. Pretorius**, Faculty of Engineering and the Built Environment, University of Johannesburg, Johannesburg, South Africa
**Prof. L. Pretorius,** Graduate School of Technology Management (GSTM), University of Pretoria, Pretoria, South Africa

**General Topics / Editors-at-large:**
**Dr P.J. Cilliers,** Hermanus Magnetic Observatory, Hermanus, South Africa
**Prof. M.A. van Wyk**, Dept. of Electrical and Information Engineering, University of Witwatersrand, Johannesburg, South Africa

**INTERNATIONAL PANEL OF REVIEWERS**
W. Boeck, Technical University of Munich, Munich, Germany
W.A. Brading, Australia
Prof. G. De Jager, Dept. of Electrical Engineering, University of Cape Town, Cape Town, South Africa
Prof. B. Downing, Dept. of Electrical Engineering, University of Cape Town, Cape Town, South Africa
Dr W. Drury, Control Techniques Ltd, United Kingdom
PD Evans, Dept. of Electrical, Electronic & Computer Engineering, The University of Birmingham, Birmingham, UK
Prof. J.A. Ferreira, Electrical Power Processing Unit, Delft University of Technology, Delft, The Netherlands
O. Flower, University of Warwick, UK
Prof. H.L. Hartnagel, Dept. of Electrical Engineering and Information Technology, Technical University of Darmstadt, Darmstadt, Germany
C.F. Landy, Engineering Systems Inc., USA
D.A. Marshall, ALSTOM T&D, France
Dr M.D. McCulloch, Dept. of Engineering Science, Oxford, United Kingdom
Prof. D.A. McNamara, University of Ottawa, Ottawa, Canada
M. Milner, Hugh MacMillan Rehabilitation Centre, Canada
Prof. A. Petroianu, Dept. of Electrical Engineering, University of Cape Town, Cape Town, South Africa
Prof. K.F. Poole, Holcombe Dept. of Electrical and Computer Engineering, Clemson University, United States of America
Prof. J.P. Reynders, Dept. of Electrical & Information Engineering, University of the Witwatersrand, Johannesburg, South Africa
I.S. Shaw, University of Johannesburg, SA
H.W. van der Broeck, Phillips Forschungslabor Aachen, Germany
Prof. P.W. van der Walt, University of Stellenbosch, Stellenbosch, South Africa
Prof. J.D. van Wyk, Dept. of Electrical and Computer Engineering, Virginia Tech, United States of America
RT Waters, UK
TJ Williams, Purdue University, USA

Additional reviewers are approached as necessary

**Published by**
SAIEE Publications (Pty) Ltd, PO Box 751253, Gardenview, 2047,
Tel. (27-11) 487-3003, Fax. (27-11) 487-3002,
E-mail: SAIEEPublications@saiee.org.za

**Additional reviewers are approached as necessary**
**ARTICLES SUBMITTED TO THE SAIEE AFRICA RESEARCH JOURNAL ARE FULLY PEER REVIEWED**
**PRIOR TO ACCEPTANCE FOR PUBLICATION**

**The following organizations have listed SAIEE Africa Research Journal for abstraction purposes:**
INSPEC (The Institution of Electrical Engineers, London); "The Engineering Index" (Engineering Information Inc.)

Unless otherwise stated on the first page of a published paper, copyright in all materials appearing in this publication vests in the SAIEE. All rights reserved. No part of this publication may be reproduced, stored in a retrieval system or transmitted in any form or by any means, electronic, magnetic tape, mechanical photocopying, recording or otherwise without permission in writing from the SAIEE. Notwithstanding the foregoing, permission is not required to make abstracts on condition that a full reference to the source is shown. Single copies of any material in which the Institute holds copyright may be made for research or private use purposes without reference to the SAIEE.

# SAIEE AFRICA RESEARCH JOURNAL – NOTES FOR AUTHORS

This journal publishes research, survey and expository contributions in the field of electrical, electronics, computer, information and communications engineering. Articles may be of a theoretical or applied nature, must be novel and must not have been published elsewhere.

### Nature of Articles

Two types of articles may be submitted:

- Papers: Presentation of significant research and development and/or novel applications in electrical, electronic, computer, information or communications engineering.
- Research and Development Notes: Brief technical contributions, technical comments on published papers or on electrical engineering topics.

All contributions are reviewed with the aid of appropriate reviewers. A slightly simplified review procedure is used in the case of Research and Development Notes, to minimize publication delays. No maximum length for a paper is prescribed. However, authors should keep in mind that a significant factor in the review of the manuscript will be its length relative to its content and clarity of writing. Membership of the SAIEE is not required.

### Process for initial submission of manuscript

Preferred submission is by e-mail in electronic MS Word and PDF formats. PDF format files should be 'press optimised' and include all embedded fonts, diagrams etc. All diagrams to be in black and white (not colour). For printed submissions contact the Managing Editor. Submissions should be made to:

The Managing Editor, SAIEE Africa Research Journal,
PO Box 751253, Gardenview 2047, South Africa.
E-mail: researchjournal@saiee.org.za

These submissions will be used in the review process. Receipt will be acknowledged by the Editor-in-Chief and subsequently by the assigned Specialist Editor, who will further handle the paper and all correspondence pertaining to it. Once accepted for publication, you will be notified of acceptance and of any alterations necessary. You will then be requested to prepare and submit the final script. The initial paper should be structured as follows:

- TITLE in capitals, not underlined.
- Author name(s): First name(s) or initials, surname (without academic title or preposition 'by')
- Abstract, in single spacing, not exceeding 20 lines.
- Text in 1½ spacing.
- List of references (references to published literature should be cited in the text using Arabian numerals in square brackets and arranged in numerical order in the List of References).
- Author(s) affiliation and postal address(es).
- Footnotes, if unavoidable, should be typed in single spacing.

### Format of the final manuscript

The final manuscript will be produced in a 'direct to plate' process. The assigned Specialist Editor will provide you with instructions for preparation of the final manuscript and required format, to be submitted directly to:
The Managing Editor, SAIEE Africa Research Journal, PO Box 751253, Gardenview 2047, South Africa.
E-mail: researchjournal@saiee.org.za

### Page charges

A page charge of R200 per page will be charged to offset some of the expenses incurred in publishing the work. Detailed instructions will be sent to you once your manuscript has been accepted for publication.

### Additional copies

An additional copy of the issue in which articles appear, will be provided free of charge to authors.
If the page charge is honoured the authors will also receive 10 free reprints without covers.

### Copyright

Unless otherwise stated on the first page of a published paper, copyright in all contributions accepted for publication is vested in the SAIEE, from whom permission should be obtained for the publication of whole or part of such material.

VOL 100 No 2
June 2009

# SAIEE Africa Research Journal

SAIEE AFRICA RESEARCH JOURNAL EDITORIAL STAFF ..... IFC

Cooperative diversity using repeat-punctured turbo codes
by J. M. Mouatcho Moualeu, H. Xu and F. Takawira ..... 34

Efficient management of clock drift in preamble sampling mac protocols for wireless sensor networks
by C. E. Tönsing and G. P. Hancke .....40

A duopoly pricing model for wireless mesh networks under congestion-sensitive users
by H. Zhu and A.Nel and W. Clarke.....48

NOTES FOR AUTHORS .....IBC

CBI electric low voltage

Eskom

# COOPERATIVE DIVERSITY USING REPEAT-PUNCTURED TURBO CODES

**J. M. Mouatcho Moualeu, H. Xu and F. Takawira**

*School of Electrical, Electronic and Computer Engineering, University of KwaZulu-Natal, King George V Avenue, Durban, 4041, South Africa. Email: {202513559, xuh, ftakaw}@ukzn.ac.za*

**Abstract:** When mobiles cannot accommodate multiple antennas due to size, hardware complexity and/or other constraints, space-time coding cannot be used to provide uplink transmit diversity. Recently, cooperative diversity has been introduced where mobiles achieve uplink transmit diversity by relaying each other's messages. A particularly powerful variation of this principle is coded cooperation which partitions the codewords of each mobile and transmits portions of each codeword through independent fading channels. Coded cooperation framework has been easily extended using turbo codes, since cooperative coding contains two codes components. It has been shown that the conventional turbo codes can be improved by repetition and puncturing. This paper presents another extension to coded cooperation. We investigate the application of repeat-punctured turbo codes in coded cooperation. The analysis and simulation results show that the proposed scheme achieves approximately 2dB gain for a 12dB inter-user channel at a BER of $10^{-4}$ order.

**Key words:** Cooperative diversity, diversity, turbo codes.

## 1. INTRODUCTION

The mobile wireless channel suffers from multipath fading, which causes the signal attenuation to vary significantly over a given transmission [1] and makes it extremely difficult for the receiver to determine the transmitted signal, unless the receiver is provided with some form of diversity. Transmit diversity methods have been studied extensively as a means to combat the deleterious effects of multipath fading in wireless fading channels [2]-[4]. Due to size, hardware complexity and/or other constraints, transmit diversity methods are not applicable to many wireless communication systems. For example in the uplink of a cellular communication system, where the size of the mobile is a limiting factor. However, most wireless systems operate in multi-user scenario. Cooperation among users has been suggested in [5]-[7][19][20], where mobiles share their antennas to achieve uplink transmit diversity. Diversity is achieved by transmitting a user's data through different paths. Coded cooperation proposed in [8] combines cooperative diversity with channel coding. In this scheme, cooperation occurs through puncturing a user's codeword such that part of the codeword is transmitted by the user itself while the remainder of the codeword is transmitted by the partner.

To avoid error propagation, detection is employed at the partner. An extension to the coded cooperation framework is presented in [9] where the application of turbo codes (TC) in coded cooperation is investigated. Turbo codes employ two recursive systematic convolutional (RSC) codes with interleaving [10]. The interleaver permutes the information bits within a frame in order to reduce the chance of both RSC encoders generating low weight parity sequences. The performance of TC improves with increasing interleaver size due to interleaver gain [11]. Increasing the interleaver size requires increasing the frame length since the interleaver size is identical to the information frame length in conventional TC, resulting in transmission delays. A simple but effective TC structure termed repeat-punctured turbo code is proposed in [12], which enables the use of interleavers of size larger than the information frame length. It is also shown, via distance spectrum analysis and computer simulations, that Repeat-Punctured Turbo Codes (RPTC) significantly outperform conventional TC, for moderate to high signal-to-noise ratios (SNR) in additive White Gaussian Noise (AWGN) channel.

In this paper, we propose a coded cooperation using repeat-punctured turbo codes in slow fading. We show that coded cooperation with RTPC outperforms turbo coded cooperation introduced in [9]. The remainder of this paper is organized as follows. In Section 2, we describe the system model and the performance analysis is provided in Section 3. The numerical results are presented in Section 4. Finally, conclusions are drawn in Section 5.

## 2. CODED COOPERATION WITH RPTC

### *2.1 System Model*

We consider a communication system, and focus on the cooperation between two users. This can be extended to a scenario with more than two users. The channels between the users and the destination (uplink) are independent of each other and independent of the channels between the users (inter-user). We assume that the inter-user channels are reciprocal. All channels are subject to flat fading. We

consider the case in which the destination or receiver maintains channel state information and employs coherent detection so that in the analysis we need only consider the fading coefficient magnitudes. Our system uses BPSK modulation, with all users having the same transmit power. For the BPSK modulation, the baseband-equivalent discrete-time signal transmitted by user $i \in \{1,2\}$ and received by user $j \in \{0,1,2\}$ $(j \neq i)$, where $j = 0$ denotes the destination, is given by

$$r_{i,j}(n) = \alpha_{i,j}(n)\sqrt{E_{b,i}}\,b_i(n) + z_j(n), \qquad (1)$$

where $E_{b,i}$ is the transmitted energy per bit for user $i$, $b_i(n) \in (-1,+1)$ is the BPSK modulated code bit at time $n$, $\alpha_{i,j}(n)$ is the fading coefficient magnitude between users $i$ and $j$, and $z_j(n)$ accounts for the effects of additive receivers noise and other forms of interference, and is modeled as zero-mean, mutually independent, white complex Gaussian random variables with variance $\sigma^2 = N_o/2$ per dimension. The fading coefficients $\alpha_{i,j}(n)$ are modeled as independent sample of Rayleigh-distributed random variable characterized by the mean-square value $\Omega_{i,j} = E_{\alpha_{i,j}}\left[\alpha_{i,j}^2(n)\right]$, where $E_x[.]$ denotes the expectation operator with respect to the random variable $x$. For slow fading, the fading coefficients remain constant over the transmission of each source block. The instantaneous received SNR for the channel between users $i$ and $j$ is defined as

$$\gamma_{i,j} = \frac{\alpha_{i,j}^2(n)E_{b,i}}{N_o}. \qquad (2)$$

For $\alpha_{i,j}(n)$ Rayleigh distributed, $\gamma_{i,j}(n)$ has an exponential distribution with mean

$$\Gamma_{i,j} = E_{\alpha_{i,j}}\left[\gamma_{i,j}(n)\right] = \Omega_{i,j}\frac{E_{b,i}}{N_j}. \qquad (3)$$

We assume the channels statistics are not changing with time, that is, $\Omega_{i,j}$ and $\Gamma_{i,j}$ are constant over $n$ for a given channel.

### *2.2 Implementation Issues*

The implementation of coded cooperation using repeat-punctured turbo codes is described here. Repeat-punctured turbo codes consist of two parallel concatenated component code encoders. The encoder of the first component code is similar to the recursive systematic convolutional encoder of conventional turbo codes. However, the second one is different from the RSC encoder of turbo code. In conventional turbo code, the information sequence of length $N$ is directly permuted by an interleaver, whereas in the case of RPTC, the information sequence of length $N$ is first repeated $L$ times and then permuted by an interleaver of size $LN$ [12]. For our scheme, we use a repeater $L = 2$. The encoder and decoder structures for each user are shown in Figs. 1 and 2.

The implementation of coded cooperation using repeat-punctured turbo codes is shown in Fig. 3. The codeword for the first frame is obtained using the first RSC. The user repeats twice the source bits of length $N$ before permuting through an interleaver of size $2N$, punctures to $N$ bits and then transmits the parity bits corresponding to the second RSC. This is done upon successful decoding of the partner.

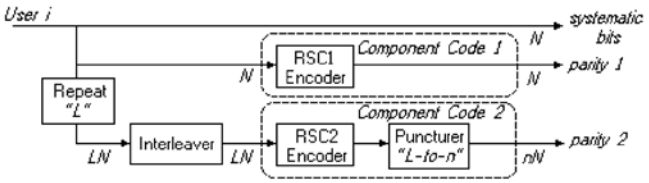


Fig. 1. RPTC encoder structure.

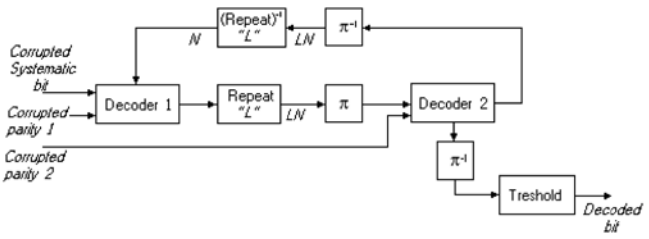


Fig. 2. Structure of the RPTC decoder.

This scheme has a fixed cooperation percentage of 33%. At the destination, the combination of the first and second frames offers the possibility of turbo decoding.

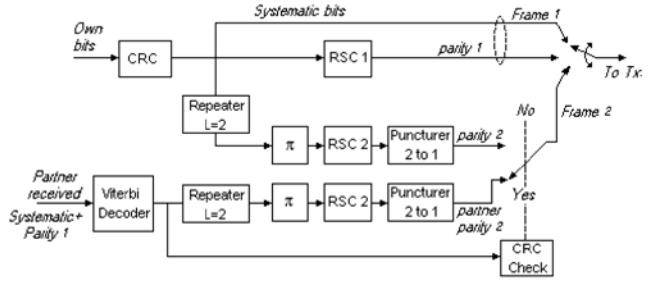


Fig. 3. Repeat-punctured turbo encoding in a coded cooperation scheme.

## 3. PERFORMANCE ANALYSIS

In this section, we provide an analysis of the coded cooperation with RPTC. First the pairwise error probabilities are derived by using the tools and techniques developed in [13]. This is done in Section 3-1. In Section 3-2, we derive the weight enumerators as in [16] and finally in Section 3-3, the upper union bounds for the end-to-end bit error probability are determined.

### *3.1 Pairwise Error Probability*

The pairwise error probability (PEP) for a coded system is the probability of detecting an erroneous codeword $e$ when codeword $c$ was transmitted. The PEP is written as [14, (12.13)],

$$P(c \to e \mid \gamma) = Q\left(\sqrt{2\sum_{n\in\eta}\gamma(n)}\right), \tag{4}$$

where $Q(x)$ denotes the Gaussian $Q$-function [15]. The set $\eta$ is the set of all $n$ for which, $c(n) \neq e(n)$, so the cardinality of $\eta$, $|\eta| = d$ ,where $d$ is the hamming distance between $c$ and $e$. For two-user cooperation, four cases arise:

a) The case of full cooperation, that is, when both users decode each other's coded bits successfully, the coded bits are divided between the two user channels. In this case, we can write (4) as

$$P(d \mid \gamma_1, \gamma_2) = Q\left(\sqrt{2d_1\gamma_1 + 2d_2\gamma_2}\right), \tag{5}$$

where $\gamma_1$ and $\gamma_2$ denote user 1 and 2's uplink channel respectively, $d_1$ and $d_2$ are the numbers of bits in the Hamming weight $d$ that are transmitted through user 1's and user 2's uplink channel. The unconditional probability is obtained by averaging (5) respectively over the fading distributions, as

$$P(d) = \int_0^\infty\int_0^\infty P(d \mid \gamma_1, \gamma_2)\, p(\gamma_1)\, p(\gamma_2)\, d\gamma_1 d\gamma_2, \tag{6}$$

where $p(x)$ is the probability density function (PDF) of $x$. The exact solution can be derived using the techniques in [14] as described in [8] and the resulting upper bound is

$$P(d) \le \frac{1}{2}\left(\frac{1}{1+d_1\bar{\gamma}_1}\right)\left(\frac{1}{1+d_2\bar{\gamma}_2}\right), \tag{7}$$

where $\bar{\gamma}_i$ is the average SNR for user $i$ 's uplink channel.

b) In the non-cooperation case, the conditional PEP is obtained by setting $d_1 = d$ and $d_2 = 0$ in (5), resulting in

$$P(d \mid \gamma) = Q\left(\sqrt{2d\gamma}\right), \tag{8}$$

and the unconditional PEP becomes

$$P(d) \le \frac{1}{2}\left(\frac{1}{1+d\bar{\gamma}}\right). \tag{9}$$

c) The case in which user 1does not successfully decodes user 2, but user 2 successfully decodes user 1, the conditional PEP for user 1 can be written as

$$P(d \mid \gamma_1, \gamma_2) = Q\left(\sqrt{2d\gamma_1 + 2d_2\gamma_2}\right). \tag{10}$$

And the unconditional PEP becomes

$$P(d) \le \left(\frac{1}{1+d\bar{\gamma}_1}\right)\left(\frac{1}{1+d_2\bar{\gamma}_2}\right). \tag{11}$$

### *3.2 Weight enumerators*

Transfer function bounding techniques studied in [16] were used to derive the union bounds of the repeat-punctured turbo codes. We start with the transition matrix as shown in (12)

$$A(L,I,D) = \begin{pmatrix} L^l I^i D^{d}_{0,0} & \cdots & L^l I^i D^{d}_{0,2^m} \\ \vdots & \ddots & \vdots \\ L^l I^i D^{d}_{2^m,0} & \cdots & L^l I^i D^{d}_{2^m,2^m} \end{pmatrix} \tag{12}$$

where $l$ is always equal to 1 for rate $1/m$, $i$ and $d$ are either 0 or 1, depending on whether the corresponding input and output bits are 0 or 1 respectively in the monomial $L^l I^i D^d$. For a given code fragment, defined by a state diagram with $2^m$ states and an $m$ bits terminated trellis path, the generating function is defined by

$$T(L,I,D) = \sum_{l\ge 0}\sum_{i\ge 0}\sum_{d\ge 0} L^l I^i D^d t(l,i,d), \tag{13}$$

where $t(l,i,d)$ denotes the number of paths of length $l$, input weight $i$ and output weight $d$ starting and

ending in the state $0^m$.

Since $I + A + A^2 + A^3 + \cdots = (I - A)^{-1}$, the transfer function can be reduced to

$$T(L,I,D) = \left[ \left( I - A(L,I,D) \right)^{-1} \right]_{0^m,0^m} \tag{14}$$

Using the recursive method explained in [16], we can determine $t(l,i,d)$ for the $(15/13)$ code fragment used for our simulations, for $l \geq 0, i \geq 0, d \geq 0$:

$$\begin{aligned}
t(l,i,d) = {} & t(l-1,i,d) + t(l-1,i-1,d-1) - t(l-6,i-5,d-5) \\
& - t(l-6,i-1,d-1) + t(l-6,i-5,d-1) + t(l-6,i-1,d-5) \\
& - t(l-7,i-5,d-1) + t(l-7,i-7,d-3) - 2t(l-7,i-5,d-5) \\
& - t(l-7,i-1,d-5) + t(l-7,i-3,d-7) - t(l-7,i-6,d-2) \\
& - t(l-7,i-2,d-6) + 2t(l-7,i-3,d-3) - 2t(l-7,i-2,d-2) \\
& + t(l-7,i,d-4) + t(l-7,i-4,d) + 2t(l-7,i-4,d-4) \\
& - t(l-8,i-8,d-4) - t(l-8,i-4,d-8) - t(l-8,i-4,d) \\
& + 2t(l-8,i-6,d-6) + 2t(l-8,i-2,d-6) + 2t(l-8,i-6,d-2) \\
& + 2t(l-8,i-2,d-2) - t(l-8,i,d-4) - 4t(l-8,i-4,d-4) \\
& + \delta(l,i,d) - \delta(l-1,i-1,d-1) - \delta(l-2,i-1,d-1) - \delta(l-3,i-1,d-1) \\
& - \delta(l-4,i-1,d-1) + \delta(l-4,i-3,d-3) - \delta(l-5,i-1,d-1) \\
& + \delta(l-5,i-3,d-3) - \delta(l-6,i-1,d-5) + 2\delta(l-6,i-3,d-3) \\
& - \delta(l-6,i-5,d-1) + \delta(l-7,i-2,d-6) - \delta(l-7,i,d-4) \\
& - \delta(l-7,i-4,d) + 2\delta(l-7,i-2,d-2) - 2\delta(l-7,i-4,d-4) \\
& + \delta(l-7,i-6,d-2).
\end{aligned} \tag{15}$$

Denote the conditional probability of producing a codeword fragment of weight $d$ given a randomly selected input sequence of weight $i$ by (16) for the first encoder

$$p(d_1 \mid i) = \frac{t(N,i,d_1)}{\sum_{d_1} t(N,i,d_1)} = \frac{t(N,i,d_1)}{\binom{N}{i}}, \tag{16}$$

and by (17) for the second encoder

$$p(d_2 \mid i) = \frac{t(LN,Li,d_2)}{\sum_{d_2} t(LN,Li,d_2)} = \frac{t(LN,Li,d_2)}{\binom{LN}{Li}}. \tag{17}$$

*3.3 Bit Error Rate Analysis*

The PEP and the weight enumerators derived in Section 3.1 and Section 3.2 will enable us to compute the end-to-end bit error probabilities. We first need to calculate the probability of operating in the cooperative mode, which can be parameterized with $\Theta = \{1,2,3,4\}$ where $\Theta = 1$ corresponds to the full cooperation case $\Theta = 2$ is the non-cooperation case, $\Theta = 3$ corresponds to the case in which user 1 does not successfully decode user 2, but user 2 successfully decodes user 1 and $\Theta = 4$ is the case in which user 1 successfully decodes user 2, but user 2 does not successfully decode user 1. For the full cooperation case, the conditional inter-user block error probability is given by

$$\begin{aligned}
P(\Theta = 1 \mid \gamma) &= \left(1 - P_{block}^{(1)}(\gamma)\right)\left(1 - P_{block}^{(2)}(\gamma)\right) \\
&\leq \left(1 - P_E^{(1)}(\gamma)\right)^B \left(1 - P_E^{(2)}(\gamma)\right)^B \\
&\leq \left(1 - BP_E^{(1)}(\gamma)\right)\left(1 - BP_E^{(2)}(\gamma)\right),
\end{aligned} \tag{18}$$

where $P_{block}(\gamma)$ is the block error rate which, using the method in [17] is bounded by

$$\begin{aligned}
P_{block}(\gamma) &\leq 1 - \left(1 - P_E(\gamma)\right)^B && (19) \\
&\leq BP_E(\gamma). && (20)
\end{aligned}$$

In (20) $B$ is the number of trellis branches in the codeword and $P_E(\gamma)$ is the error event probability. For a $1/n$ convolutional code, $B$ equals the uncoded block length $K$. It can be shown that $P_E(\gamma)$ is bounded by [18]

$$P_E(\gamma) \leq \sum_{d=d_{\min}}^{\infty} a(d) P(d \mid \gamma), \tag{21}$$

where $d_{\min}$ is the minimum distance of the code and $a(d)$ is the number of error events with Hamming distance $d$. The conditional inter-user block error probability for the other cases can be derived in a similar method as in (18) and is omitted here. The end-to-end bit error rate probabilities is calculated using the unconditional inter-user block error probability $P(\Theta)$ and given by

$$P(\Theta) = \int_{\gamma} P(\Theta \mid \gamma).p(\gamma) d\gamma. \tag{22}$$

Using (20) yields loose bounds in the case of slow fading as shown in [17]. The limit-before-average technique is used in (19) to give tight bounds on the block error probability. For the case of full cooperation, this tight upper bound is obtained by

$$\begin{aligned}
P(\Theta = 1) \leq {} & \int_{\gamma} \left(1 - \min\left[1, \sum a_1(d) P(d \mid \gamma)\right]\right)^B \\
& \times \left(1 - \min\left[1, \sum a_2(d) P(d \mid \gamma)\right]\right)^B p(\gamma) d\gamma.
\end{aligned} \tag{23}$$

The other case can be obtained in the same way.

The overall end-to-end BER is obtained by averaging the unconditional BER over the four possible cases discussed above, as shown

$$P_b = \sum_{i=1}^{4} P_b(\Theta) P(\Theta = i), \qquad (24)$$

where $P_b$ is the BER. The conditional BER uses a bound similar to the bound in [18, (4.4.8)]

$$P_b(\gamma, \Theta) \le \sum_{d=d_{\min}}^{\infty} a(d) P(d \mid \gamma), \qquad (25)$$

where $a(d)$ is given by

$$a(d) = \underbrace{\sum_{i} \sum_{d_1} \sum_{d_2}}_{d=i+d_1+d_2} \frac{i}{k} \binom{k}{i} P(d_1 \mid i) P(d_2 \mid i). \qquad (26)$$

The unconditional BER is obtained by averaging (25). As discussed above, tight bounds on the unconditional BER are obtained using the limit-before-average described in [17]. The unconditional BER is thus given by

$$P_b(\Theta) \le \int_{\gamma} \min\left[\frac{1}{2}, P_b(\gamma, \Theta)\right] p(\gamma) d\gamma. \qquad (27)$$

## 4. NUMERICAL RESULTS

In this section, we plot some examples of the upper bounds on the unconditional BER $P_b$ using the limit-before-average technique described in [17] and compare them with the simple average technique. We also compare the BER bounds with simulation results for the RPTC code implementation of coded cooperation. For all the simulations, we use a source block code of $N = 128$ bits. We employ a rate $1/2$, eight-state constituent codes with generator polynomial $G(1, 15/13)_{octal}$ and a repeater $L = 2$. The cooperation percentage is $33\%$. The overall code rate is $1/3$.

The convergence of the union bound on the bit error probability using the simple average method and the one obtained from the limit-before-average method is shown in Fig. 4. It is seen that the limit-before-average union bound on the bit error probability converges rather fast, whereas the simple average method calculated as the sum as the of the average pairwise error probabilities does not. The summation in (24) where the upper limit corresponds to $d_{\max}$ is truncated such that only the error events having the total distance $d = d_1 + \ldots + d_L \le d_{\max}$ are taken into account.

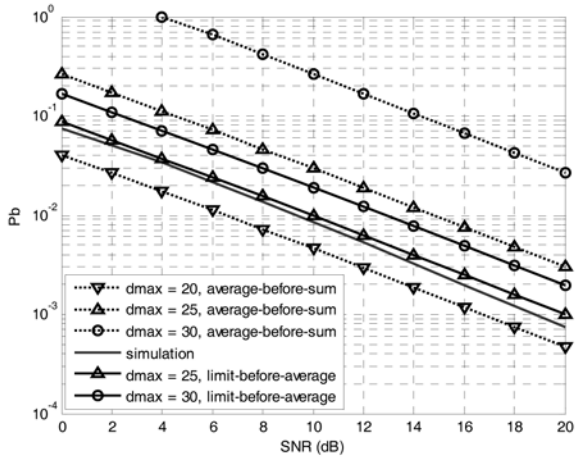


Fig. 4. Union bounds on the bit error probability $P_b$ for different values of $d_{\max}$.

Fig. 5 compares the performance of the turbo coded cooperation [9] and the repeat-punctured turbo coded cooperation in slow fading, with an overall rate $1/3$. We note that the repeat-punctured turbo coded cooperation performs almost 2dB better than the turbo coded cooperation for higher uplink SNR, both for 6dB and 12dB inter-user channel.

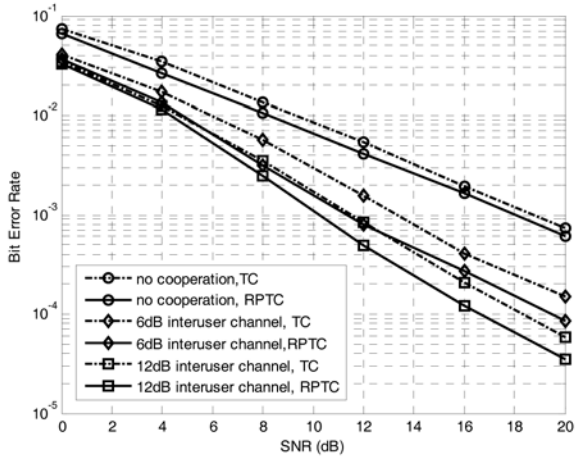


Fig. 5. Comparison of turbo coded cooperation and repeat-punctured turbo coded cooperation in slow fading.

Fig. 6 shows the theoretical BER bounds versus computer simulations for the repeat-punctured turbo coded cooperation scheme in slow fading with reciprocal inter-user channels of various qualities. The level of cooperation is 33% and the users have the same uplink channels. Combining [16] and [17] yields tight bounds on the BER as shown in Fig. 6.

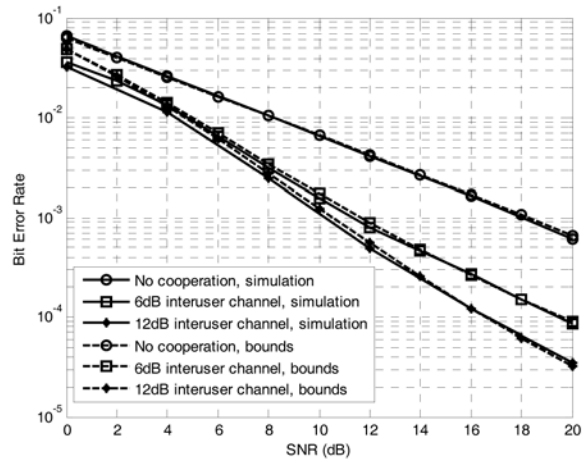


Fig. 6. Performance in slow Rayleigh fading with 33% cooperation, equal uplink SNR and reciprocal inter-user channels of the repeat-punctured turbo code with coded cooperation.

## 5. CONCLUSION

In this paper, cooperative diversity with repeat-punctured turbo codes is presented. Simulation results of this scheme are discussed in Section-4 as well as the theoretical bounds on the bit error probability. Prior to that, a comparison of the turbo coded cooperation developed in [9] and the repeat-punctured turbo coded cooperation is presented. It is noted that the new scheme outperforms the turbo coded cooperative scheme by almost 2dB for higher uplink for different qualities of the inter-user channel. The theoretical bounds of the RPTC with coded cooperation closely match the simulation results.

## 6. ACKNOWLEDGEMENTS

This work was supported in part by Alcatel-Lucent and Telkom as part of the centres of Excellence Programme.

## 7. REFERENCES

[1] T. S. Rappaport, Wireless Communications: Principles and Practice, Upper Saddle River, N.J: Prentice-Hall, 1996.

[2] N. Balaban and J. Salz, "Dual diversity combining and equalization in digital cellular mobile radio," *IEEE Trans. Veh. Technol.,* vol. 40, pp. 342-354, May 1991.

[3] G. J. Foschini Jr., "Layered space-time architecture for wireless communication in a fading environment when using multiple antennas," *Bell Labs Tech. J.,* pp. 41-59, Autumn, 1996.

[4] G. J. Foschini Jr. and M. J. Gans, "On limits of wireless communication in a fading environment when using multiple antennas," *Wireless Personal Commun.,* pp. 311-335, March 1998.

[5] A. Sendonaris, E. Erkip, and B. Aazhang, "User cooperation diversity-Part I: System description," *IEEE Trans. Commun,* vol. 51, no. 11, pp. 1927–1938, November 2003.

[6] A. Sendonaris, E. Erkip, and B. Aazhang. "User cooperation diversity-Part II: Implementation aspects and performance analysis," *IEEE Trans. Commun., vol. 5* 1, no. 11, pp.1939–1948, November 2003.

[7] J. N. Laneman, G. W. Wornell, and D. N. C. Tse , "An efficient protocol for realizing cooperative diversity in wireless networks," in *Proc. IEEE International Symposium on Information Theory (ISIT),* Washington, DC., June 2001, pp. 294.

[8] T. E. Hunter and A. Nosratinia, "Diversity through Coded Cooperation," *IEEE Trans. On Wireless Comm.*, vol. 5, no. 2, pp 283-289, February. 2006

[9] M. Janani, A. Hedayat, T. E. Hunter, and A. Norastinia, "Coded cooperation in wireless communications: Space-time transmission and iterative decoding," *IEEE Trans. Signal Processing,* vol. 52, no. 2, pp. 362-371, February 2004.

[10] C. Berrou, A. Glavieux "Near Optimum error correcting coding and decoding: Turbo codes," *IEEE Trans. Commun.*, vol. 44, pp. 1261-1271, October 1996.

[11] S. Benedetto and G. Montorsi, "Unveiling turbo codes: Some results on parallel concatenated coding schemes," *IEEE Trans. Inform. Theory*, vol. 42, no. 2, pp. 409-428, March 1996.

[12] Y. Kim, J. Cho, K. Cheun, "Improving the performance of turbo codes by repetition and puncturing," *JCCI 2004*, April 2004.

[13] J. W. Craig, "A new, simple, and exact result for calculating the probability of error for two dimensional signal constellations," in *Proc. IEEE MILCOM*, McLean, VA, October 1991, pp. 571-575.

[14] M. K. Simon and M. S. Alouini, *Digital Communication over Fading Channels: A Unified Approach to Performance Analysis*. New York: John Wiley and Sons, 2000.

[15] J. K. Proakis, *Digital Communications*, 3rd ed. New York: McGraw-Hill, 1995.

[16] D. Divsalar, S. Dolinar and F. Pollara, "Transfer function bounds on the performance of turbo codes," *Telecom and Data Acquisition Progress Report 42-122*, JPL, August 1995

[17] E. Malkamaki and H. Leib, "Evaluating the performance of convolutional codes over block fading channels," *IEEE Trans. Inform. Theory*, vol. 45, no. 5, pp. 1643-1646, July 1999.

[18] A. Viterbi and J. K. Omura, Principles of Digital Communication Coding, New York: McGraw-Hill, 1979.

[19] E. Beres and R. Raviraj, "Selection cooperation in multi-source cooperative networks," *IEEE Trans. Wireless Commun.*, vol.7, No.1, pp. 118-127, January 2008.

[20] S. S. Ikki and M. H. Ahmed, "On the performance of Amplify-and-Forward cooperative diversity with the $N^{th}$ best relay selection scheme," in *Proc. IEEE ICC*, Dresden, Germany, 2009.

# EFFICIENT MANAGEMENT OF CLOCK DRIFT IN PREAMBLE SAMPLING MAC PROTOCOLS FOR WIRELESS SENSOR NETWORKS

**C. E. Tönsing* and G. P. Hancke****

** Department of Electrical, Electronic and Computer Engineering, University of Pretoria, Pretoria, 0002, South Africa, E-mail: christoph.tonsing@gmail.com*
*** Department of Electrical, Electronic and Computer Engineering, University of Pretoria, Pretoria, 0002, South Africa, E-mail: g.hancke@ieee.org*

**Abstract:** In this paper, the design of an energy-efficient Medium Access Control (MAC) protocol for low traffic Wireless Sensor Networks (WSNs) is presented. The protocol, Dynamic Preamble Sampling MAC (DPS-MAC), is based on the existing preamble sampling MAC layer solutions for WSNs. Unlike its predecessors, DPS-MAC does not cater for the worst case clock drift but rather, it dynamically adjusts its operation to the clock drift experienced between any two communicating nodes. In this way, the energy previously expended on overcoming the problem of clock drift is reduced, leading to longer node and network lifetimes.

**Key words:** Clock drift, MAC protocol, Preamble Sampling, Wireless Sensor Networks.

## 1. INTRODUCTION

Wireless Sensor Networks (WSNs) form an area of interest that has rapidly expanded in the recent past. A WSN is a collection of many small devices called sensor nodes. Each node is generally capable of performing some type of environment sensing (e.g. temperature, humidity etc.), processing the sensed data and wirelessly communicating with neighboring nodes, usually for forwarding data in a hop by hop fashion from one node to the next towards a sink node or base station node. At the base station/sink node, all the data received from the surrounding nodes can be further processed or stored as necessary.

Typical applications of WSNs include battlefield surveillance, intruder detection, wildlife observation, monitoring of agricultural processes, wildfire detection, home automation and many more. Essentially all of the application areas of WSNs have the common requirements that the sensor networks should be void of fixed infrastructure, should be dynamically deployable, should operate autonomously without human assistance/intervention, and should remain active for long periods of time. To meet these requirements, a WSN node must be autonomous itself, carrying with it a supply of energy (e.g. a battery) or the ability to scavenge energy from its surrounding environment (e.g. a solar panel). It is thus imperative that each node be able to survive for as long as possible with a highly limited supply of energy. The decisive design challenge underlying all types of WSNs is therefore energy efficiency. Other challenges such as small size, low cost etc. may or may not be crucial depending on the specific application. However, without energy efficiency, most of the other design challenges can never be met. A node cannot be made small if it needs a large battery or solar panel to operate. Also, a WSN cannot be made low cost if the maintenance of the network requires battery replacements.

The challenge of making WSNs energy efficient is a task that needs to be dealt with at every level of the network and every step of the design process. Raghunathan *et al*. [1] give an excellent overview of energy efficiency in WSNs. The authors make the important observation that the main consumer of energy in a node with current state of the art technology is the active wireless transceiver. The use of the transceiver must therefore be meticulously controlled so as to prevent energy wastage from prematurely rendering a node useless in the field.

It is generally accepted that the method of energy conservation is to have the transceiver of a node active for only very short periods of time for transmission and reception. During the remainder of the time, the transceiver, or even the entire node, is powered down. This method of operation is referred to as duty cycling and the process of sleep and wakeup cycles is controlled and coordinated among nodes by the Medium Access Control (MAC) layer of the communications protocol stack. The MAC protocol is thus a crucial part of an energy-efficient WSN design.

This paper deals with the design of a new energy-efficient MAC protocol with the goal of extending the useful lifetime of a WSN. The rest of this paper is organized as follows. Section 2 deals with related work in the existing literature. A general overview of existing WSN MAC protocols is given, followed by a closer analysis of the specific protocols that form the design basis for the new protocol. The design of the new MAC protocol is then discussed in Section 3. Section 4 gives the results of the protocol simulation and finally, Section 5 concludes the paper.

## 2. RELATED WORK

### *2.1 WSN MAC Protocols Overview*

From the current literature pertaining to the topic of WSN MAC protocols, it is clear that there are two main types of WSN MAC protocols, namely schedule-based protocols (e.g. Time Division Multiple Access (TDMA)-type protocols) and contention-based protocols (e.g. Carrier Sense Multiple Access (CSMA)-type protocols). Since it has become clear that WSNs of varying kinds exist and will be devised in the future, it must be kept in mind that different applications will likely require very different hardware and protocols. This is expressly pointed out in a number of articles, such as the extensive WSN overview by Sadler [2].

As a very general classification, it can be stated that the properties of schedule-based MAC protocols lend them suitable for applications where the traffic patterns are deterministic and the topology static. Furthermore they mostly require tight time synchronization among nodes and are thus more suitable for medium to high traffic applications where a relatively constant stream of data is available to keep node clocks synchronized. Lastly they are suitable to be used in networks where the nodes gather into a clustered topology, with the cluster-head being in control of the scheduling functions. A few examples of schedule-based MAC protocols are LEACH [3], TRAMA [4], DE-MAC [5], and EMACS [6].

As far as contention-based MAC protocols are concerned, their properties make them generally suitable for use in bursty traffic scenarios due to the fact that they do not follow a schedule. They are also suitable for use in low traffic scenarios due to their ability to operate at low duty cycles. Traditional contention-based protocols such as the IEEE 802.11 MAC protocol are useful for low latency scenarios. However, such protocols have high energy consumption. To counter this problem, the duty-cycled MAC protocol was introduced. The classical and extensively quoted WSN MAC protocol in this category is S-MAC [7] which has resulted in a number of derivatives and adaptations (e.g. T-MAC [8] or DSMAC [9]). Among contention-based protocols, another group of duty-cycled protocols are those employing preamble sampling to establish communication between two nodes. Some prominent examples of this protocol group are WiseMac [10], CSMA-MPS [11] and B-MAC [12].

### *2.2 Design Basis*

It is apparent from the literature that the specific area of low traffic WSNs (i.e. WSNs where nodes transmit data relatively infrequently) has not been dealt with exhaustively. The preamble sampling family of MAC protocols shows suitability for such WSNs as these protocols can easily operate at low duty cycles.

Low duty cycled contention-based MAC protocols generally operate as follows. Each node in the network has a short listen slot during which time its transceiver is in listening mode to determine whether there is any incoming data from a neighboring node. If not, the transceiver is switched off again until the next listen slot. If there is incoming data, the node continues to receive until the data packet is fully delivered and then switches off the transceiver again. The time between successive listen slots, $T_w$, is the same for all nodes in a network; however, the listen slot start times are not synchronized among nodes. They are in fact randomly distributed. Therefore, if node A wants to send a data packet to a neighboring node B, it needs to know when this destination node will have its next listen slot. To do this, node A maintains a table with information of its one-hop neighbors. This table contains each neighboring node's address, as well as the time stamp since last communication with that node. From this time stamp and $T_w$, node A can calculate the time at which node B will have its next listen slot. In an ideal scenario, the sender will thus know the exact point in time at which the intended destination node will wake up and send the data at that instant. The destination node will wake up to listen and immediately start receiving the data. The reason why the ideal scenario cannot be achieved is summed up in the term *clock drift*. There is not a single clock which can maintain perfect time. This applies especially to cheap sensor nodes with cheap quartz crystals as frequency source. A crystal oscillator frequency tolerance of $\pm\Theta$ can cause timing errors on the order of $\pm\Theta L$, where L is the time since last clock resynchronization. Values of $\Theta$ for crystal oscillators can be in the region of 10-100 ppm (parts per million).

Preamble sampling protocols overcome the problem of clock drift by sending a preamble before the actual data packet to make sure that the destination's listen slot is "hit". In other words, if node A wants to send a packet to a neighboring node B, it must send a preamble until it is sure that node B has switched on its transceiver and is listening for incoming data. Node B thus notices the incoming preamble during its listen slot and continues to listen until the actual data packet is delivered immediately after the preamble. In this way, the preamble may be viewed as waking up the destination node, enabling the actual data to be delivered reliably.

Some preamble sampling protocols like B-MAC do not keep track of neighboring nodes' listen schedules. In this case, node A starts sending a preamble as soon as data becomes available for transmission to node B. The preamble is sent for $T_w$ seconds, followed by the actual data. In this way, node A is sure that node B had a listen slot during the preamble transmission and continued listening until the data was delivered.

In order to shorten the preamble sending time and thus

save energy, the WiseMac protocol keeps track of neighboring nodes' listen schedules. Node A can thus calculate an estimation of B's next listen slot start, $t_{est}$, using the time stamp of last communication and $T_w$ as mentioned above. If the maximum frequency tolerance of the nodes' crystal oscillators is given by $\pm\Theta$, the authors of the WiseMac protocol show in [10] that the estimated listen slot start, $t_{est}$, will be in error by a maximum of $\pm 2\Theta L$ seconds. Therefore, node B may in fact start its listen slot $2\Theta L$ seconds before or after $t_{est}$. To ensure that node B's listen slot is "hit", node A should start sending the preamble $2\Theta L$ seconds before $t_{est}$ and continue to send it for $2\Theta L$ seconds after $t_{est}$, a total of $4\Theta L$ seconds. Of course, if the time since last communication, L, becomes large enough so that $4\Theta L > T_w$, then the preamble need only be sent for $T_w$ seconds. In summary, the maximum preamble length in seconds is given by $T_{preamble} = \min(4\Theta L, T_w)$. For appropriate values of L, nodes using the WiseMac protocol can thus save significant energy compared to using a MAC protocol that does not keep track of neighboring nodes' listen schedules.

The CSMA-MPS protocol is based on WiseMac and took some ideas from STEM [13], [14] as well. The authors of CSMA-MPS point out in [11] that the WiseMac protocol sends out a continuous preamble and the preamble length, $T_{preamble}$, is fixed prior to sending the preamble. Thus, even if the destination node, node B, starts its listen slot right at the beginning of the preamble, it still has to listen to the entire length of the preamble to receive the actual data straight afterwards. The STEM protocol takes a different approach, as its preamble consists of short alternating transmit and receive slots. During the transmit slot, a packet containing the destination node's address is sent out. During the receive slot, the source node listens for a preamble acknowledgement (ACK) packet. If no preamble ACK packet is received, the next preamble packet is sent out, and so forth. When node B wakes up for its listen slot and detects an incoming preamble packet from node A, node B responds with a preamble ACK packet to acknowledge its readiness to receive data from node A. Node A can thus stop sending the preamble and instead send the actual data. The CSMA-MPS protocol uses this same preamble format and on average halves the preamble sending time compared to WiseMac. In this way, CSMA-MPS improves on the energy efficiency and network lifetime of WiseMac.

It was noted that even though protocols like WiseMac and CSMA-MPS directly address the problem of clock drift, this problem has always been represented as a single value, $\Theta$, the maximum frequency tolerance of the oscillator hardware. These protocols thus always assume worst case clock drift, whereas the properties and characteristics of the $\Theta$ value have not been investigated further. The DPS-MAC protocol discussed in this paper builds specifically on the CSMA-MPS protocol as the most energy efficient existing preamble sampling MAC protocol. Some basic properties of the frequency tolerance value are exploited so as to shorten preamble sending times and allow DPS-MAC to achieve improved energy efficiency compared to its predecessor.

### *2.3 Clock Drift*

*Overview:* So far, the quality of a clock source has been described by a single value, $\Theta$, the frequency tolerance of the clock source. However, the quality of a clock in fact consists of two distinct concepts, namely *accuracy* and *stability* [15]. The degree to which a crystal oscillator is *accurate* is the degree to which the average frequency at which it oscillates is close to its specified resonant frequency. On the other hand, the degree to which an oscillator is *stable* is the degree to which the frequency output of the oscillator varies from its average value over time. Thus, if a microcontroller uses a quartz crystal oscillator, the timing errors, or clock drift, that can be expected by the microcontroller consists of two parts. Firstly, a fixed frequency offset will cause its time to drift from actual time at a fixed rate, say $\Theta_{ave}$. This is the clock *inaccuracy* and is caused mainly by variations in the exact shape and cut of the quartz crystals at manufacturing time. Secondly, the crystal's frequency output may vary over time due to various sources of *instability*, causing uncertainty in the microcontroller's time reference at any point in time.

A fixed frequency offset and the resulting timing errors that increment at a fixed rate can easily be compensated for if the average drift rate, $\Theta_{ave}$, is known. Therefore, the uncertainty caused by frequency instability presents a greater problem to clock synchronization and the magnitude of this problem is now investigated more closely.

*Clock instability:* Intuitively, the procedure to evaluate a clock's quality would be to repetitively measure the frequency of the clock and then analyze the data. The average value of all the measurements would indicate the inaccuracy of the clock (fixed offset) and the standard deviation would indicate the instability of the clock (random fluctuations). There is a problem with this approach though, since clock frequency cannot be measured instantaneously, but needs an averaging interval $\tau$ in which to count the number of clock cycles so as to calculate the frequency for that interval $\tau$. It turns out that the standard deviation is ill-defined for such a set of measurements as it shows dependency on the length of interval $\tau$ and in certain situations, the standard deviation value does not converge to a sensible value [16]. To solve this problem, different measures have been proposed to characterize clock stability. The specification which has been recommended by the IEEE to characterize clock stability in the time domain is referred to as the Allan deviation which is the square root of the Allan variance [17]. It is denoted by $\sigma_y(\tau)$. A detailed explanation of what it represents can be found in [16].

The reason why the Allan deviation is such a useful measure is because it is straightforward to convert the

Allan deviation to the timing errors that can be expected from an oscillator. This is achieved as follows. If a clock is perfectly synchronized and set at a point in time, then $\tau$ seconds later, the expected time error of the clock is simply calculated as $\tau\sigma_y(\tau)$ [17]. The two coordinates of a point on the $\sigma_y(\tau)$ plot are thus multiplied together and this gives the remaining time error that can be expected once the average time error, caused by a fixed frequency offset, has been removed. In other words, this value represents the expected time error standard deviation. Using the above procedure, a graph of the expected time error standard deviation for quartz crystal oscillators is generated as shown in Figure 1, by using the data from the $\sigma_y(\tau)$ plot in Figure A1 of [18].

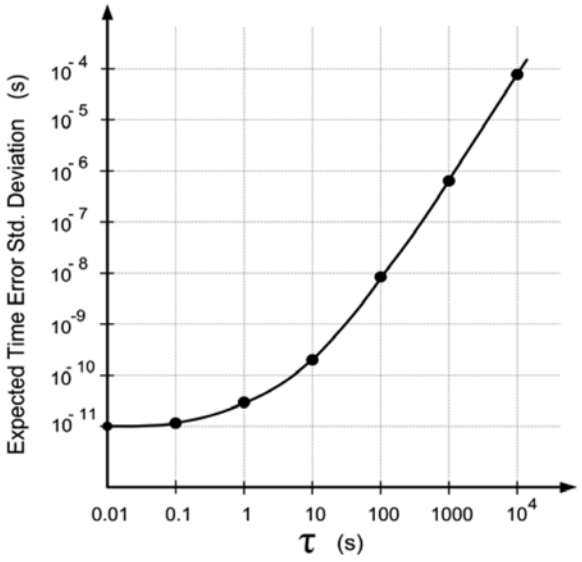


Fig 1: Expected time error standard deviation vs. synchronization interval $\tau$ for quartz crystals.

To demonstrate these observations, take as example a microcontroller which implements a clock function. Suppose that the microcontroller's crystal oscillator has an average frequency inaccuracy given by $\Theta_{ave}$ = 20 ppm = $20\times10^{-6}$. At time zero the microcontroller's time is synchronized perfectly to a hypothetical perfect time reference. After $\tau$ = 100 seconds, the time error caused by the fixed frequency offset in the crystal is given by $\Theta_{ave} \times \tau = 2\times10^{-3}$ seconds. On the other hand, using the graph in Figure 1 for $\tau$ = 100 seconds shows that the time error caused by clock instability is only approximately $9\times10^{-9}$ seconds. In this case, the random time error caused by clock instability is more than five orders of magnitude smaller than the time error caused by the fixed frequency offset. In fact, as seen in Figure 1, up to a resynchronization interval of $\tau$ = 1000 seconds, the time error due to instability is on the order of less than 1 µs. As $\tau$ increases, processes such as random frequency walk, component aging as well as temperature changes may increase the effects of frequency instability [17].

The observations that have been made regarding clock drift are exploited in the design of the DPS-MAC protocol as discussed next.

## 3. PROTOCOL DESIGN

As has been mentioned, the Dynamic Preamble Sampling MAC (DPS-MAC) protocol is based on the CSMA-MPS MAC protocol. The three operational states of the DPS-MAC protocol are as follows, keeping in mind that the first two of these states are the same as in the CSMA-MPS protocol.

### *3.1 State 1 - Unsynchronized*

When a node is first powered up, it has no knowledge of the listen schedules of its surrounding nodes. Each node simply begins its own listen schedule upon startup i.e. it enters a short listen period every $T_w$ seconds. For each node, the scheduling of this listen slot is independent of any of its surrounding nodes and there is no synchronization of listen schedules amongst nodes. When such a node, say node A, needs to transmit data to one of its neighboring nodes, it starts the transmission process immediately. The transceiver is first switched on, entering a wake-up (WU) mode until it is fully functional. Then, a carrier sense (CS) operation is done to determine whether the medium is busy or not. If the medium is detected as busy, the transmission attempt is rescheduled after a short random time in the interval $[T_w/2, T_w]$. If the medium is found idle, node A starts sending the preamble. After a maximum of $T_w$ seconds, the destination node, node B, will have had its listen slot and in response sent a preamble ACK packet, telling node A to send the actual data. After receiving the data, node B responds with a final ACK packet. Node B measures the time difference, $\Delta t_{l\text{-}r}$, between when its listen slot started, $t_{listenB}$, and when it actually received the first valid preamble packet, $t_{rxpreambleB}$. This value is returned to node A in the preamble ACK packet. In this way, node A knows exactly the time at which node B started its listen slot, and stores this value with node B's entry in the neighbor table as the last time of communication, $t_{lastB}$. The next time a communication must occur with node B, node A can operate in the second state.

### *3.2 State 2 – Slot Estimate Available*

Having had a previous successful communication with node B, node A can roughly estimate the time at which node B will have its next listen slot, $t_{estB}$, by simply adding $T_w$ repetitively to $t_{lastB}$ until a value greater that the current time is obtained. Each node in the network also knows the maximum frequency tolerance of the crystal oscillators used on the nodes, $\Theta_{max}$. As explained previously for the WiseMac protocol, node A will thus start sending the preamble $2\Theta_{max}L_B$ seconds before $t_{estB}$, where $L_B = t_{estB} - t_{lastB}$. In fact, CSMA-MPS adds a short random time, $t_{rand}$, to prevent similarly synchronized neighbors from sending data to node B at the same time, causing a collision. This random time is given as $t_{rand} = kT_{rx\text{-}tx}$, where k is a uniform random integer in the interval [0, N], N being the number of entries in the neighbor table, and $T_{rx\text{-}tx}$ is the receive-transmit switching time of the transceiver hardware, a constant. Thus, the

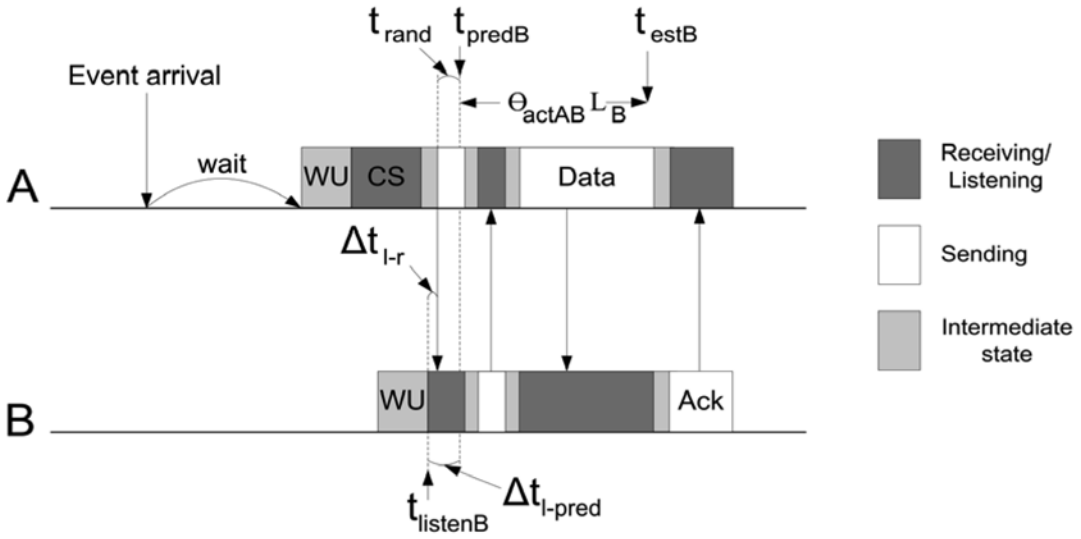


Fig 2: The operation of the DPS-MAC protocol in the third state where a clock drift estimate to the destination node is available.

time at which node A actually starts sending a preamble to B is given by $t_{txA} = t_{estB} - 2\Theta_{max}L_B - t_{rand}$. If before starting the transmission, node A detects the medium busy during the CS operation, the transmission is rescheduled for node B's next listen slot. If the medium is idle, node A starts sending the preamble. Upon reception of the first valid preamble packet, node B again measures the time difference $\Delta t_{l\text{-}r}$ and includes this value in the preamble ACK packet. From this value, node A again calculates the time at which node B started its listen slot, $t_{listenB}$, and stores this again as the last time of communication with node B, $t_{lastB}$. Furthermore, node A also knows the time at which it originally estimated node B would start its listen slot, $t_{estB}$. From this point on, DPS-MAC extends the functionality of CSMA-MPS. Node A calculates $\Delta t_{l\text{-}est} = t_{listenB} - t_{estB}$ as the difference in time between when node B actually started listening and when node A estimated node B would start listening. From this, node A can calculate the actual clock drift that occurred between the two nodes in the time since the last communication as $\Theta_{actAB} = \Delta t_{l\text{-}est}/L_B$. This value is stored in node A's neighbor table entry for node B and the next time a communication must occur with node B, node A can operate in the third state.

### *3.3 State 3 – Clock Drift Estimate Available*

From the previous protocol state, node A was able to calculate the actual clock drift that it observed with node B, $\Theta_{actAB}$. As was shown in the section on clock instability, the biggest portion of $\Theta_{actAB}$ is in fact a stable value, namely two fixed frequency offsets, one each in node A and node B's crystal oscillators. The $\Theta_{actAB}$ value will thus remain stable enough so as to accurately predict node B's next listen slot. To do this, node A again calculates $L_B = t_{estB} - t_{lastB}$, the time since last communication with node B. Node A then predicts node B's next listen slot start as $t_{predB} = t_{estB} + \Theta_{actAB}L_B$ as shown in Figure 2. Note that $\Theta_{actAB}$ has a negative value in the example in Figure 2, therefore $t_{predB}$ occurs before $t_{estB}$. The unstable portion of the $\Theta_{actAB}$ value is the sum of the instabilities in node A and node B's crystal oscillator output. As was shown, the uncertainty in each node's oscillator output due to instabilities is on the order of $\tau\sigma_y(\tau)$ seconds. In the worst case, the sum of the uncertainties of both nodes' oscillators will thus be on the order of $2\tau\sigma_y(\tau)$ seconds. As seen in Figure 1, up to a synchronization interval of $\tau$ = 1000 seconds, $2\tau\sigma_y(\tau)$ is less than $2\times10^{-6}$ seconds. Therefore, even if nodes A and B last communicated 1000 seconds (approximately 16 minutes) ago, node A can predict the start of node B's next listen slot, $t_{predB}$, as described above, and only be in error by approximately 2 µs. In terms of a transceiver operating at a bit rate of 1 Mbps, 2 µs is the equivalent of 2 bits being transmitted. It is not expected that WSNs will use transceivers operating at bit rates much higher than 1 Mbps. In fact, most practical implementations so far have operated at much lower bit rates. In this context, a time slot start prediction error of 2 µs can be viewed as insignificant. As $\tau$ increases above 1000 seconds, the uncertainty in the listen slot prediction grows larger, due to component aging, random frequency walk etc. and thus, DPS-MAC requires a node to send a very short keep-alive packet to a neighboring node if no communication has occurred with that node for more than 15 minutes.

As is seen in Figure 2, node A again adds a short random time, $t_{rand}$, to its prediction of node B's listen slot start. The magnitude of $t_{rand}$ is the same as in the second state. Furthermore, when node B has received the first valid preamble packet, it again calculates the time difference $\Delta t_{l\text{-}r}$ and includes this value in the preamble ACK packet sent back to A. Node A calculates the time at which node B started listening, $t_{listenB}$, and node A also knows $t_{predB}$, the time at which it predicted node B would listen. From these values, A calculates $\Delta t_{l\text{-}pred} = t_{listenB} - t_{predB}$. Since node A already has a drift estimate for node B, the value

of $\Delta t_{l\text{-}pred}$ includes the short term instability of the two nodes' oscillators on the one hand, but also any long term changes in node A and B's oscillator outputs due to component aging, environmental changes etc. and thus, it cannot be ignored. Node A uses the $\Delta t_{l\text{-}pred}$ value to update its clock drift estimate for node B by calculating $\Theta_{actAB} = \Theta_{actAB} + \Delta t_{l\text{-}pred}/L_B/2$. This calculation essentially sets the next value of $\Theta_{actAB}$ to the average of its current value and the newly measured value. In this way, DPS-MAC easily deals with long term changes in the crystal oscillators' frequency outputs.

*3.4 Summary of Protocol Features*

From the above basic operational description, it can be seen that DPS-MAC builds on the existing CSMA-MPS protocol and extends this protocol's energy savings by dynamically adjusting to the clock drift experienced between any two neighboring nodes. No additional protocol overhead is required to sustain this functionality. In fact, DPS-MAC is designed to reduce the length of preambles compared to its predecessors. Furthermore, DPS-MAC is fully distributed and operates autonomously at each node. No clustering is required and nodes are not grouped hierarchically. Also, the protocol does not rely on complex calculations and can be implemented on resource constrained hardware of different kinds.

## 4. SIMULATION AND RESULTS

The DPS-MAC protocol was compared to its predecessor, CSMA-MPS, using simulation. The comparison was done on the one hand to verify the DPS-MAC protocol design, and on the other hand to demonstrate the energy savings of DPS-MAC over CSMA-MPS, if any. The details of the simulation as well as its results are discussed next.

*4.1 Simulation Details*

Simulations were performed using the OMNeT++ platform, version 3.2. On top of this, the Mobility Framework simulator, version 1.0-a-6 was used. The state machines of the DPS-MAC and CSMA-MPS protocols were fully implemented in this framework. Every single state in which the transceiver of a node may operate was modeled in the simulation, including startup and intermediate states, transmitting, active receiving, passive listening and off states. In this way, the total time spent by a node in any of the possible communication states at any point in time was accurately measured for each node in the simulation. From these timing values, the energy consumption of each node in the simulation network was calculated.

The simulated network consisted of 50 nodes, randomly distributed in a 400 m × 400 m square area. A sink node was located at the centre of the area, collecting the data from all the nodes in the network. Upon startup, the sink node sent a broadcast packet to all its neighbors, with a hop count (HC) set to zero. Each of the recipients incremented the received HC by one and then forwarded the packet to its own neighbors, away from the sink node. At the end of this startup procedure, each node knew its distance in hops from the sink node. During normal operation, whenever a node had a packet to transmit (either generated by itself or received from an upstream neighbor) it forwarded the packet to the downstream neighbor (a neighbor with smaller HC) whose next listen slot occurred soonest. In this way, data always travelled towards the sink node and routing loops were prevented.

The simulation provided no external synchronization amongst the nodes. Each node chose a random point in time to start its listen slot schedule upon startup. From then on, the communication process occurred as explained in the above description of the two protocols' states of operation. The listen slot period, $T_w$, was set at 10 seconds, whereas each node was simulated as generating a packet regularly every 15 minutes. The simulation duration was set to 1 day.

The transceiver model used in the simulations is based on the CC2400 radio from Chipcon [19]. The transceiver was simulated to operate at a bit rate of 1 Mbps.

*4.2 Results*

Numerous simulation tests were performed to demonstrate the performance of DPS-MAC in comparison to CSMA-MPS under various operating conditions. The test which demonstrates most clearly the difference between the two protocols is a simulation using various maximum frequency tolerance values, $\Theta_{max}$, for the crystal oscillators of the nodes in the network. Values of $\Theta_{max}$ between 10 ppm and 80 ppm were simulated.

The graph showing the average transmitting time per node for the two simulated protocols for various values of the maximum frequency tolerance is shown in Figure 3 below.

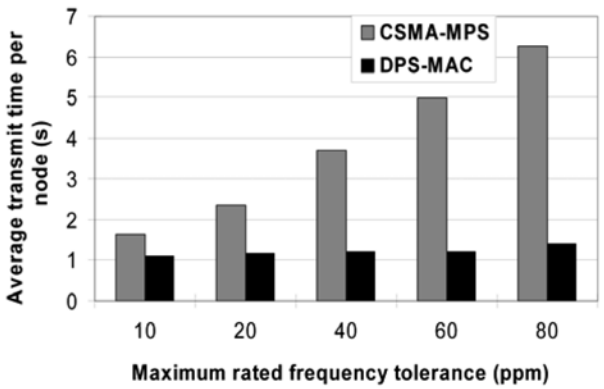


Fig 3: Comparison of the average transmit time per node for CSMA-MPS and DPS-MAC for various maximum frequency tolerance values. The simulation time is 1 day.

CSMA-MPS always starts sending a preamble $2\Theta_{max}L$ seconds before the neighbor's listen slot is estimated to start, where L is the time since last communication. Therefore, intuitively, the larger the value of $\Theta_{max}$, the longer the preamble transmission will be. DPS-MAC on the other hand dynamically adjusts its predictions of the neighbor's listen slot to the actual observed clock drift and not the worst case clock drift. The transmission time is therefore largely independent of $\Theta_{max}$. These expectations are confirmed by the results in Figure 3.

Taking into account the duration of the transceiver in each of the states, the average power consumption per node can be obtained as shown in Figure 4 below.

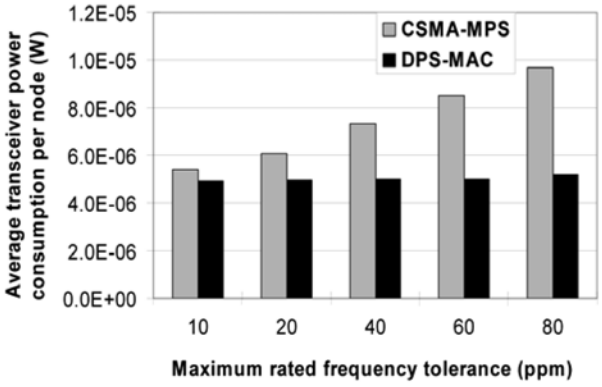


Fig 4: The average transceiver power consumption of DPS-MAC and CSMA-MPS for various maximum frequency tolerance values.

Finally, the transceiver energy savings of DPS-MAC over CSMA-MPS is given in Figure 5 below. It is clear that as the quality of the clock increases (i.e. the frequency tolerance rating decreases), the energy savings of DPS-MAC over CSMA-MPS decrease. However, even when using high quality crystal oscillators with frequency tolerance ratings of around 20 ppm, DPS-MAC still demonstrates an increase in transceiver energy savings of approximately 18 % over CSMA-MPS.

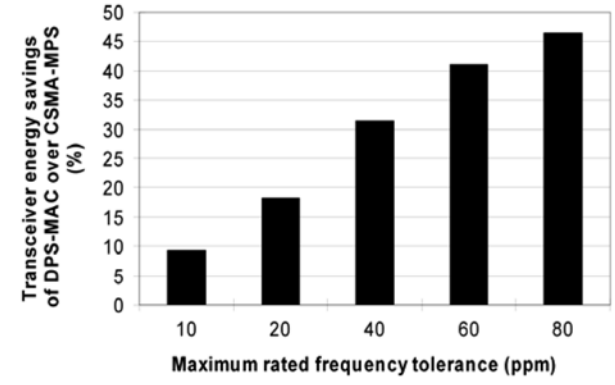


Fig 5: The transceiver energy savings of DPS-MAC over CSMA-MPS for various maximum frequency tolerance values.

## 5. CONCLUSION

A preamble sampling MAC protocol for WSNs, called DPS-MAC, has been presented in this paper. By exploiting some characteristics of the frequency tolerance ratings of crystal oscillators, DPS-MAC is able to cause a significant reduction in the duration of preamble transmission compared to its predecessors. DPS-MAC is aimed specifically at application in low traffic WSNs and can be used to achieve longer network lifetimes in such WSNs, in this way contributing to making such networks more feasible.

## 6. REFERENCES

[1] V. Raghunathan, C. Schurgers, S. Park and M. B. Srivastava: "Energy-aware wireless microsensor networks," *IEEE Signal Processing Mag.*, vol. 19, no. 2, pp. 40-50, Mar. 2002.

[2] B. M. Sadler: "Fundamentals of Energy-Constrained Sensor Network Systems," *IEEE A&E Systems Mag.*, vol. 20, no. 8, pp. 17-35, Aug. 2005.

[3] W. R. Heinzelman, A. Chandrakasan and H. Balakrishnan" "Energy-Efficient Communication Protocol for Wireless Microsensor Networks," in *2000 Proc. Ann. Hawaii International Conference on System Sciences*, pp. 1-10.

[4] V. Rajendran, K. Obraczka and J. J. Garcia-Luna-Aceves: "Energy-efficient, collision-free medium access control for wireless sensor networks," in *2003 Proc. SenSys Conf.*, pp. 181-192.

[5] R. Kalidindi, L. Ray, R. Kannan and S. Iyengar: "Distributed Energy Aware MAC Layer Protocol for Wireless Sensor Networks," in *2003 Proc. International Conf. on Wireless Networks*, pp. 282-286.

[6] L. F. W. van Hoesel, T. Nieberg, H. J. Kip and P. J. M. Havinga: "Advantages of a TDMA based, energy-efficient, self-organizing MAC protocol for WSNs," in *2004 Proc. IEEE Vehicular Technology Conf.*, vol. 3, pp.1598-1602.

[7] W. Ye, J. Heidemann and D. Estrin: "An Energy-Efficient MAC Protocol for Wireless Sensor Networks," in *2002 Proc. INFOCOM Conf.*, pp. 1567-1576.

[8] T. van Dam and K. Langendoen: "An Adaptive Energy-Efficient MAC Protocol for Wireless Sensor Networks," in *2003 Proc. SenSys Conf.*, pp. 171-180.

[9] P. Lin, C. Qiao and X. Wang: "Medium access control with a dynamic duty cycle for sensor

networks," in *2004 Proc. IEEE WCNC Conf.*, vol. 3, pp. 1534-1539.

[10] A. El-Hoiydi and J.-D. Decotignie: "WiseMAC: an ultra low power MAC protocol for the downlink of infrastructure wireless sensor networks," in *2004 Proc. ISCC Symp.*, pp. 244 – 251.

[11] S. Mahlknecht and M. Böck: "CSMA-MPS: a minimum preamble sampling MAC protocol for low power wireless sensor networks," in *2004 Proc. IEEE Workshop on Factory Comm. Systems*, pp. 73-80.

[12] J. Polastre, J. Hill and D. Culler: "Versatile low power media access for wireless sensor networks," in *2004 Proc. SenSys Conf.*, pp. 95-107.

[13] C. Schurgers, V. Tsiatsis, S. Ganeriwal and M. Srivastava: "Optimizing Sensor Networks in the Energy-Latency-Density Design Space," *IEEE Trans. on Mobile Computing*, vol. 1, pp. 70-80, March 2002.

[14] C. Schurgers, V. Tsiatsis and M. B. Srivastava: "STEM: Topology management for energy efficient sensor networks," in *2002 Proc. Aerospace Conf.*, pp 3-1099 - 3-1108.

[15] J. R. Vig and A. Ballato: *Ultrasonic Instruments and Devices*. Academic Press Inc., USA, 1999, ch. 7.

[16] D. W. Allan: "Time and Frequency (Time-Domain) Characterization, Estimation, and Prediction of Precision Clocks and Oscillators," *IEEE Transactions on Ultrasonics, Ferroelectrics, and Frequency Control*, vol. UFFC-34, no. 6, pp. 647-654, Nov. 1987.

[17] J. R. Vig: (2006, April). Quartz Crystal Resonators and Oscillators for Frequency Control and Timing Applications - A Tutorial (Rev. 8.5.2.3) [Online]. Available: http://www.ieee-uffc.org/freqcontrol/tutorials/vig2/tutorial2.ppt

[18] D. W. Allan, N. Ashby, and C. C. Hodge: "The Science of Timekeeping," Hewlett Packard Company, Application Note 1289, Jun. 1997.

[19] Chipcon AS. (2006, March). CC2400 datasheet (Rev. 1.5) [Online]. Available: http://www.chipcon.com

# A DUOPOLY PRICING MODEL FOR WIRELESS MESH NETWORKS UNDER CONGESTION-SENSITIVE USERS

**H. Zhu*, A. Nel† and W. Clarke‡**

* *Department of Electrical and Electronic Engineering Science, University of Johannesburg, P.O. Box 524, Auckland Park, 2006, South Africa E-mail: hailingz@uj.ac.za*

† *Department of Electrical and Electronic Engineering Science, University of Johannesburg, P.O. Box 524, Auckland Park, 2006, South Africa E-mail: andren@uj.ac.za*

‡ *Department of Electrical and Electronic Engineering Science, University of Johannesburg, P.O. Box 524, Auckland Park, 2006, South Africa E-mail: willemc@uj.ac.za*

**Abstract:** The development of Wireless Local Area Network (WLAN) technologies offers a novel platform for IP-based service resale via Wireless Mesh Networks (WMNs) that provide high network coverage and lower infrastructure cost. In this IP-based service resale business, the Access Point (AP) providers set their pricing policies as IP-based service resellers to maximize their profits, while the resale-users (end users of the WMNs) who are price- and quality-of-service (QoS)- sensitive, respond to AP providers' pricing policies by controlling their usage. In this paper we study a two AP providers' price competition in a WMN. The two AP providers offer IP-based service for possibly different prices and QoS in terms of mean packet delay. The resale-users' choice between the APs is based on their compensated utility. We consider a two stage game among the two AP providers and their resale-users. In stage 1, the AP providers set their prices to maximize their profits respectively. In stage 2, given the prices and QoS offered by both AP providers, the resale-users decide which AP to seek service from or opt out of both APs. Then the game returns to stage 1, in which both AP providers adjust their optimal prices based on the decisions of the resale-users to seek equilibrium among themselves and their resale-users. With this game theoretical approach, we develop an analytical framework to find the Nash equilibrium points from which two APs and resale-users would not move from.

**Key words:** pricing, game theory, queue theory.

## 1. INTRODUCTION

Recently, both the engineering and economic research communities have devoted large efforts to understand the Internet economics. Pricing has been studied as one of significant topics in the Internet economics because both the service providers' profits and the utilization of the networks are highly affected by it. A number of researches have shown that pricing can be viewed as a better control mechanism by which a service provider can communicate with its users and give them incentive to use the network resource efficiently. However, the majority of pricing research focuses on a monopolistic setting, in which the only service provider who deals with a multitude of individual consumers is big enough to affect the entire market.

In the deregulated telecommunications industry, especially in the competitive wireless data service market, customers have more freedom and the ability to choose their own providers as compared to a monopolized environment. The customers can leave their current service provider and subscribe to another provider at any time they want. The behavior of migrating from one service provider to another is called churning. There are many factors that influence customer churning. They include marketing, advertisement and promotional packages offered by the service providers, resource management policies, network coverage and reliability, pricing, service features offered, QoS, and so on [1].

In such an oligopoly, both users and providers are small parts of the market and everyone's behavior affects the pricing. In this paper, we investigate a duopoly pricing model which could be used for such communication service competitions using reselling IP-based service over Wireless Mesh Networks (WMNs) as an example.

Since WMN technology requires only low capital expenditure, it has been viewed as an opportunity to expand markets for telecommunication services to empower local communities and to expand economic capacity and commerce in rural areas [2]. With high network coverage and lower infrastructure cost, WMNs offer a platform for IP-based service resale. In its most general form as shown in Fig. 1, a WMN interconnects stationary and/or mobile users and provides Internet access as well as communications within the network. The nodes connected to the Internet are called access points (APs). In the WMN, the objectives of most end users would be to access the Internet at a reasonable cost. In this sense, the AP providers, who officially subscribe to an upstream Internet Service Provider (ISP), can be viewed as IP-based services resellers to resell their Internet access to the end users within the WMN. Since the upstream ISPs will not be able to monitor resold traffic within the WMN in order to bill the end users, the AP providers need to set their pricing policy to bill the end users with the intent to maximize their profit. On the other hand, the end users as buyers of the resold IP-based services are called resale-users. They can get Internet service or VoIP telephony by only paying

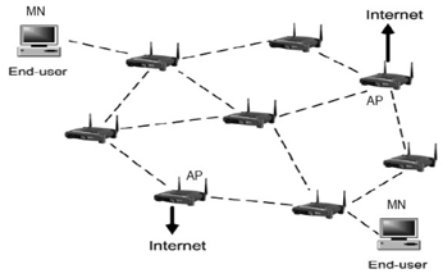


Fig 1: Basic Mesh-based Internet Access Model.

for their usage rather than paying for high subscription fees. Therefore, the relationship between an end user and an AP provider is that of a consumer-supplier model. The economics of the provision of such services have substantially different pricing characteristics - bordering on a perfect marginal cost only analysis that implies very great elasticity of supply.

To provide sufficient access bandwidth in a WMN, multiple APs need to be deployed within a certain area to provide Internet connectivity. It is more flexible for resale-users to choose among these APs based on the level of satisfaction they perceive. According to the current design of WMN architectures, a resale-user's requests will be routed to one AP automatically so that the data flows generated by the resale-user can take the most appropriate route, i.e., based on minimum hop count or QoS (in terms of bandwidth, end-to-end delay or other QoS metrics). However, from the resale-user's point of view, besides QoS, the price is also an important consideration when the resale-user selects an AP for Internet service delivery.

It has been well accepted that the current wireless data network models are flawed, in the sense that they fail to capture [1]:

- The utility of the services and network from the user's perspective;
- The impact of user demands on revenue utility from the service providers perspective.

Even though the current design of architectures, algorithms and protocols for WMNs does take users' QoS requirement into account, price competition among AP providers is not taken into consideration. We believe that in the presence of competition among multiple AP providers with different prices resource distributions within the network would be affected significantly. This would in turn affect the engineering design of WMNs. In our pricing model, we assume that resale-users can choose an AP on their own based on the quoted price and the perceived QoS instead of just being directed automatically to a certain AP by routing protocols.

The vast majority of research on price optimization and revenue management has focused on the monopolist

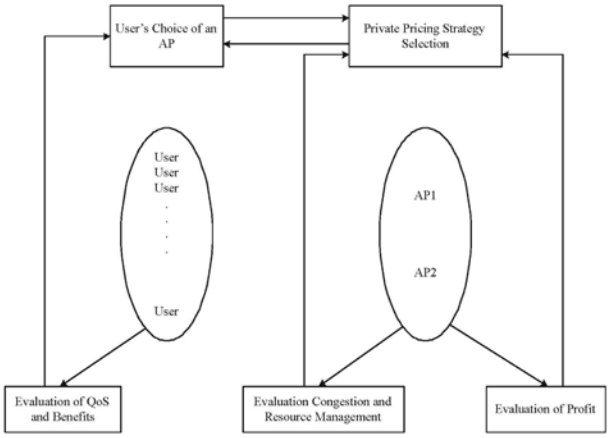


Fig 2: Pricing Model for two AP Providers.

problem. A monopolist who deals with a multitude of individual consumers is big enough to affect the entire market. Consumers therefore react to the monopolist by maximizing their welfare at the price the monopolist decides to charge. While in an oligopoly, both consumers and providers are small parts of the market. Therefore they have to take everyone else's behavior into account.

In this paper, we discuss a duopoly model involving competition between two AP providers with asymmetric costs. In such a duopoly, An AP provider's demand depends on its price, its cost and its competitor's price, cost and demand. However, both AP providers have no knowledge of the other's price, cost and demand. Therefore, the resale-users reactions to both AP providers' prices are the key factors for the AP providers to set their prices. This can be modeled as a two stage non-cooperative game: first, in stage 1, the AP providers set their prices to maximize their profits respectively. In stage 2, given prices of both AP providers, the resale-users decide whether or not to make use of the IP-based services, and if so, from which AP provider. The resale-users respond to these two AP providers by choosing the best price and QoS combination that can maximize their compensated utility. Then the game returns to stage 1, in which both AP providers adjust their prices based on the decisions of the resale-users to reach an equilibrium. As shown in Fig. 2, through this sequential decision-making process, the AP providers can capture the dynamic of resale-user behavior by exploiting the reactions of the resale-users to both AP providers' prices and QoS.

The paper is organized as follows. The basic model for the pricing game under two AP providers competition is described in Section 2.. In Section 3., we analyze the two APs competition model with resale-users' utility and develop a duopoly modeling framework. Section 4. derives analytical results for optimal price. Section 5. shows how the two AP providers with differing costs set their prices and illustrates that Nash equilibrium points exist through a numerical example. Section 6. concludes the paper.

## 2. THE BASIC MODEL

In this section, we present the basic model for the pricing game under two AP providers competition based on the work of [3], which addresses the question of duopoly with demand-dependent quality. Suppose there are two AP providers: AP1 and AP2 in a market competing to maximize individual profit. Assume the AP1 and AP2 set prices $p_1$ and $p_2$ respectively for per packet transmission, and the costs for providing per packet transmission are $c_1$ and $c_2$ respectively. Let the profit of AP1 and AP2 be denoted as $\Pi_1$ and $\Pi_2$ respectively. $\Pi_i$ is a function of the price charged for per packet, $p_i$, and the AP$i$'s cost, $c_i$.

Assume the behavior of all resale-users are identical and economically rational, so we can view all the requests as being from the same resale-user and simply use the singular word "resale-user". When a resale-user joins AP$i$ ($i = 1,2$), he/she receives gross utility $V_i$. Consider each AP as a system that can only serve a finite population of potential resale-users. The gross utility that the resale-user obtains depends partly on QoS. Obviously, generally speaking, the larger the number of resale-users subscribe to an AP, the lower the gross utility the resale-users can obtain. Given the prices offered by the AP providers, the resale-user's decision to subscribe to which AP is the determining factor in this two AP providers competition game.

A strategy for the resale-user has three options: subscribing to AP1; subscribing to AP2; opting out of both of them. From the resale-user's point of view, choosing which AP depends on his/her compensated utility, $V_i - p_i$ (utility minus price). First of all, if the compensated utilities that the user receives from both APs are negative, the user will choose to submit neither of them. Then, if the compensated utilities that a resale-user receives from one AP or both of them are positive, the resale-user will choose the AP from which he/she receives the higher compensated utility. In other words, the resale-user's strategy strongly depends on the price difference and the QoS performance difference between these two AP providers.

In [3], Gibbens *et al*. suggest that the utility experienced by a user has three components: a positive benefit $V$ which is independent of which ISP the user has joined; a dis-benefit, depending on the degree of congestion of the network provided by ISP$i$, $K_i$, and the user's preference for congestion, $\theta$. Thus, the utility of a user with a preference $\theta$ from joining ISP$i$ can be denoted as $U(\theta, i) = V - \theta K_i - p_i$. For analytical simplicity, Gibbens *et al*. [3] further assume that congestion on a network is defined as the number of users divided by the capacity of the network and given by $K_i = Q_i/C_i$, where $Q_i$ is the mass of users on the ISP$i$'s network and $C_i$ is the network capacity.

However, there are some drawbacks in the assumptions that are contained in this functional form for utility. Firstly, the assumption that the congestion function is linear may not be very realistic even though it captures the feature that the degree of congestion increases with the number of users. In reality, the effect of congestion will be negligible at low usage levels, while rising sharply beyond some critical level. Secondly, even though the hypothetical parameters, such as $V$ and $\theta$, do simplify the theoretical analysis in [3], this game theoretical model can just provide a theoretical analysis framework, which is impossible to implement practically. The first and most important reason is that it is difficult to determine the values for these hypothetical parameters. Another reason is that this game theoretical model is a complete information game while realistically it is impossible for a service provider to know the private information, such as capacity, about opponent service providers.

Actually, the utility model that Gibbens *et al*. suggest is similar to the concept of compensated utility in [4]. Without loss of generality, the compensated utility curves can be defined as:

$$U = V(y) - p, \qquad \text{with} \quad V(y) = y^{-\theta}, \tag{1}$$

where $V(\bullet)$ is gross utility and $\theta > 0$. To simplify the calculation, we choose $\theta = 1$. Thus, $U = 1/y - p$

The resale-user's gross utility is associated with QoS. However, QoS may take many different forms, such as response time, bit-error rate, packet delay, and so forth. For the purpose of facilitating analysis, mean packet delay, $ED$, is used to determine the utility experienced by a resale-user in this paper. Clearly, the mean packet delay is affected by the number of resale-users who subscribe to the same AP. Then the resale-user's gross utility is denoted as $V(ED) = 1/ED$, and the compensated utility is denoted as $U(ED) = 1/ED - p$. $V(ED)$ decreases with its argument $ED$.

Suppose that mean packet delays for AP1 and AP2 are $ED_1$ and $ED_2$ respectively. Denote $V_1(ED_1)$ and $V_2(ED_2)$ as the resale-user's gross utility for AP1 and AP2 respectively. Thus,

- if $V_1(ED_1) - p_1 < 0$ and $V_2(ED_2) - p_2 < 0$, the resale-user will opt out of both APs;
- if $V_1(ED_1) - p_1 > V_2(ED_2) - p_2 > 0$, the resale-user will subscribe to AP1;
- if $V_2(ED_2) - p_2 > V_1(ED_1) - p_1 > 0$, the resale-user will subscribe to AP2;
- only if $V_1(ED_1) - p_1 = V_2(ED_2) - p_2 > 0$, the resale-user is indifferent between AP1 and AP2.

In the situation in which the indifference relation

$$V_1(ED_1) - p_1^* = V_2(ED_2) - p_2^* \tag{2}$$

holds, there is no incentive for a resale-user to unilaterally change his/her strategy. In other words, the resale-user derives no benefit from switching to another AP because switching does not increase his/her compensated utility. Therefore, the pair of prices $(p_1^*,\ p_2^*)$, which also maximize

$\Pi_1$ and $\Pi_2$ simultaneously, is a Nash equilibrium. In equilibrium, both AP providers have no unilateral incentive to change their prices which could lead to an increase or decrease in the resale-users' compensated utility and create an incentive for the resale-user to change his/her strategies.

## 3. DUOPOLY MODEL

In a duopoly, each AP provider has knowledge about its own cost, quoting price and resale-user's response to its quoting price but does not have knowledge about its rival's cost, price and the resale-user's response to its rival's price.

We first assume that there are $N$ independent resale-users in this duopoly. All the resale-users generate information packets that they feed into the system after they submit to an AP. The resale-users who submit to the same AP share a First-In-First-Serve (FIFS) queue. To simplify the analysis, we model this FIFS queue as an M/M/1 queue [5], in which each resale-user generates packets according to a Poisson process with mean rate $\lambda$, and the service times of individual packet are i.i.d. exponentially distributed with mean $\mu^{-1}$. Thus, the mean packet delay for AP$i$ is:

$$ED = \frac{1}{\mu - \lambda N E_i(p_i)}, \tag{3}$$

where $E(p_i)$ is the expectation of the acceptance for the price $p_i$. Note that (3) only holds provided that $\mu > \lambda N E(p_i)$. In a game theoretic sense, we are making the assumption that a resale-user is a perfectly rational consumer who has no memory to influence future decisions of which AP to subscribe.

In [6] Jagannathan *et al.* suggest a parameterized customer behavior model for customer's willingness-to-pay to a given price using a Pareto distribution of customer capacity to pay. Every customer has the capacity to pay based on a Pareto distribution with scale $b$ and shape $\alpha$, where all customers have capacities at least as large as $b$ and $\alpha$ determines how the capacities are distributed. It is reasonable to assume that resale-users' willingness-to-pay is associated with their capacities to pay. Therefore, the expectation of acceptance for a given price $p_i$ is:

$$E_i(p_i) = \begin{cases} 1 - \frac{\alpha_i}{\alpha_i+\delta_i}(\frac{p_i}{b_i})^{\delta_i} & 0 \le p_i \le b_i; \\ \frac{\delta_i}{\alpha_i+\delta_i}(\frac{b_i}{p_i})^{\alpha_i} & p_i > b_i, \end{cases} \tag{4}$$

where shape $\alpha_i$, scale $b_i$ and user-willingness elasticity $\delta_i$ are determined by AP$i$ based on its own observation. Different APs should have different values of these parameters. Since an AP provider can observe the resale-users' acceptance to the quoted price online, these parameters can be learned using an adaptive algorithm suggested by Jagannathan *et al.* in [6] from the observed acceptance rate for a given price. In fact, the process of learning these parameters is a dynamic process with an aim to adjust the quoted price in line with the change of the resale-user's compensated utility. The objective of dynamically learning these parameters is to capture the time-varying feature of customer behavior.

Then the expression for the resale-user's compensated utility $U_i$ with AP$i$ can be written as:

$$U_i = V_i(ED_i) - p_i = 1/ED_i - p_i = \mu - \lambda N E_i(p_i) - p_i \tag{5}$$

Meanwhile, the profit function for AP$i$ per unit time, $\Pi_i$, is given by:

$$\Pi_i = \lambda N E_i(p_i)(p_i - c_i) \tag{6}$$

## 4. THE PRICE SELECTION PROBLEM

The AP provider will determine its price such that its profit is maximized. The profit of AP$i$ is maximized when the first order condition

$$\frac{\partial \Pi_i}{\partial p_i} = 0.$$

There are two cases need to be discussed:

- **CASE 1**: When $p_i > b_i$, $E_i(p_i) = \frac{\delta_i}{\alpha_i+\delta_i}(\frac{b_i}{p_i})^{\alpha_i}$. Then

$$\Pi_i(p_i) = \lambda N \frac{\delta_i}{\alpha_i+\delta_i}(\frac{b_i}{p_i})^{\alpha_i}(p_i - c_i) \tag{7}$$

  Differentiating (7) with respect to $p_i$,

$$\Pi_i'(p_i) = \lambda N \frac{\delta_i {b_i}^{\alpha_i}}{\alpha_i+\delta_i}(\frac{\alpha_i c_i}{{p_i}^{\alpha_i-1}} - \frac{\alpha_i - 1}{{p_i}^{\alpha_i-2}}). \tag{8}$$

  We then obtain $\Pi_i{}'(p_{i_{opt}}) = 0$ when $p_{i_{opt}} = \frac{\alpha_i c_i}{\alpha_i - 1}$.
  Differentiating again and studying the expression for $\Pi_i''(p_i)$, we find that when $p_{i_{opt}} = \frac{\alpha_i c_i}{\alpha_i - 1}$,

$$\Pi_i''(p_{i_{opt}}) = \lambda N \frac{\alpha_i \delta_i {b_i}^{\alpha_i}}{\alpha_i+\delta_i}[\frac{\alpha_i - 1}{p_i^{\alpha_i+1}} - \frac{c_i(\alpha_i+1)}{p_i^{\alpha_i+2}}] < 0. \tag{9}$$

  Therefore, $\Pi_i(p_i)$ is maximized with respect to $p_i$ when $p_{i_{opt}} = \frac{\alpha_i c_i}{\alpha_i - 1}$.

- **CASE 2**: When $0 \le p_i \le b_i$, $E_i(p_i) = 1 - \frac{\alpha_i}{\alpha_i+\delta_i}(\frac{p_i}{b_i})^{\delta_i}$. Then

$$\Pi_i(p_i) = \lambda N[1 - \frac{\alpha_i}{\alpha_i+\delta_i}(\frac{p_i}{b_i})^{\delta_i}](p_i - c_i) \tag{10}$$

  Differentiating (10) with respect to $p_i$, we get

$$\Pi_i{}'(p_i) = \lambda N[1 + \frac{\alpha_i c_i \delta_i}{(\alpha_i+\delta_i){b_i}^{\delta_i}} p_i^{\delta_i - 1} - \frac{\alpha_i(\delta_i+1)}{(\alpha_i+\delta_i){b_i}^{\delta_i}} p_i^{\delta_i}]. \tag{11}$$

  The second derivative is

$$\Pi_i{}''(p_i) = \lambda N \frac{\alpha_i \delta_i p_i^{\delta_i - 2}}{(\alpha_i+\delta_i){b_i}^{\delta_i}}[c_i(\delta_i - 1) - p_i(\delta_i + 1)] \tag{12}$$

We assume that an AP provider will set its price greater than or at least equal to its cost $c_i$ since an AP provider's prime concern is cost recovery. Thus $p_i \geq c_i > \frac{c_i(\delta_i-1)}{\delta_i+1}$ or $c_i(\delta_i-1)-p_i(\delta_i+1)<0$, which implies that $\Pi_i^{''}(p_i)<0$ in the range of $c_i \leq p_i \leq b_i$. Therefore, it is clear that $\Pi_i(p_i)$ is strictly concave in the region $c_i \leq p_i \leq b_i$. Moreover, it can be inferred from (11) that as $\Pi_i^{''}(p_i)<0$, $\Pi_i(p_i)$ also contains at least one maximization point in the range of $c_i \leq p_i \leq b_i$.

Clearly, there is at least one maximization point in the range of $c_i \leq p_i \leq b_i$ and $p_i > b_i$ respectively. Thus, solving the following maximization problem gives the optimal price at which the AP$i$ maximizes its profit:

$$\max \Pi_i(p_i) = \begin{cases} \lambda N[1-\frac{\alpha_i}{\alpha_i+\delta_i}(\frac{p_i}{b_i})^{\delta_i}](p_i-c_i) & c_i \leq p_i \leq b_i; \\ \lambda N \frac{\delta_i}{\alpha_i+\delta_i}(\frac{b_i}{p_i})^{\alpha_i}(p_i-c_i) & p_i > b_i. \end{cases} \tag{13}$$

Since a resale-user has three options: subscribing to AP1, subscribing to AP2 or opting out of both of them, $\sum_{i=1}^{2} E_i(p_i)$ must be smaller than or equal to 1. Note that here $E_i(p_i)$ is the acceptance rate at which AP$i$'s expected profit is maximized. In other words, only if AP$i$ ensures the acceptance rate $E_i(p_i)$, can the best payoff be achieved by choosing the optimal price $p_{i_{opt}}$.

Combining the constraint condition $\sum_{i=1}^{2} E_i(p_i) \leq 1$ with (2), (10) and (13), the optimal price $p_{i_{opt}}$ that maximizes AP$i$'s excepted profits must satisfy:

$$\max_{i\in\{1,2\}} \Pi_i(p_i) = \begin{cases} \lambda N[1-\frac{\alpha_i}{\alpha_i+\delta_i}(\frac{p_i}{b_i})^{\delta_i}](p_i-c_i) & c_i \leq p_i \leq b_i \\ \lambda N \frac{\delta_i}{\alpha_i+\delta_i}(\frac{b_i}{p_i})^{\alpha_i}(p_i-c_i) & p_i > b_i, \end{cases}$$
$$\text{subject to } U_1 = U_2 > 0 \text{ and } E_1(p_1)+E_2(p_2) \leq 1. \tag{14}$$

However, (14) is difficult to solve mathematically. To investigate Nash equilibrium in our model, we provide a numerical example in the following section.

## 5. NUMERICAL EXAMPLE

As proved, for $\Pi_i$ defined in (14) there is at least one maximization point within the ranges of $c_i \leq p_i \leq b_i$ and $p_i > b_i$ respectively. To determine which one is the maximization point for all $p_i$, we have to study the expression for $\Pi_i$ further.

Fig. 3 shows the maximum of the profit function $\Pi_i$ and the corresponding optimal price for different assumed values of scale parameter, $b$, with $\alpha = 4$, $\delta = 3$ and $c_i = 5$. Fig. 4 further plots the expected profit per unit time for different assumed values of willingness elasticity parameter, $\delta_i$, with $\alpha_i = 4$, $b_i = 8$ and $c_i = 5$. As can be observed, the willingness elasticity parameter, $\delta_i$, has no affect on the value of the optimal price, $p_{i_{opt}}$. Without loss of generality

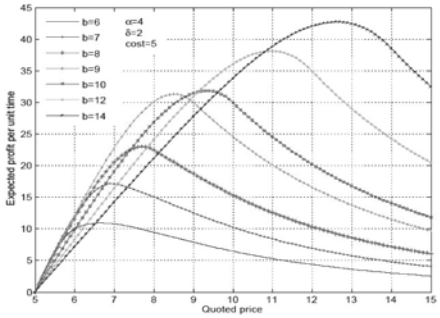


Fig 3: Expected profit per unit time versus quoted price for different scale parameter $b$.

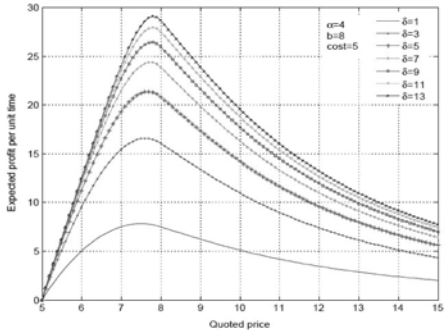


Fig 4: Expected profit per unit time versus quoted price for different willingness elascity parameter δ.

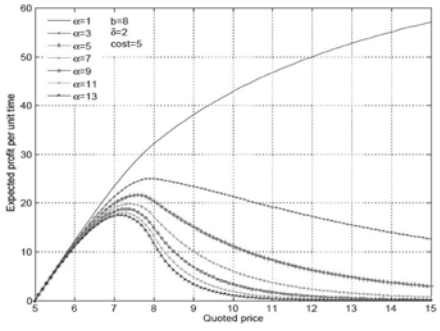


Fig 5: Expected profit per unit time versus quoted price for different willingness elascity parameter α.

and so as to simplify the analysis, we assume $\delta_i = 2$ for both APs.

Fig. 5 plots the expected profit per unit time for different assumed values of shape, $\alpha_i$, with $b_i = 8$, $\delta_i = 2$ and $cost_i = 5$. It can be seen that when $\alpha_i = 1$ the profit function is a strictly increasing function while when $\alpha_i > 1$ the value of the optimal price, $p_{i_{opt}}$, is sightly affected by the value of shape, $\alpha_i$. For instance, when $\alpha_i = 3$ the corresponding $p_{i_{opt}}$ is 7.9 while when $\alpha_i = 13$ the corresponding $p_{i_{opt}}$ is 6.9.

Consider a more general form of profit function with $\delta_i = 2$

as following:

$$\max \Pi_i(p_i) = \begin{cases} \lambda N[1-\frac{\alpha_i}{\alpha_i+2}(\frac{p_i}{b_i})^2](p_i-c_i) & c_i \le p_i \le b_i; \\ \lambda N \frac{2}{\alpha_i+2}(\frac{b_i}{p_i})^{\alpha_i}(p_i-c_i) & p_i > b_i. \end{cases} \tag{15}$$

The corresponding optimal price is:

$$p_{i_{opt}} = \begin{cases} \frac{1}{3}(c_i + \sqrt{c_i^2 + \frac{3(\alpha_i+2)}{\alpha_i}b_i^2}) & c_i \le p_i \le b_i; \\ \frac{\alpha_i}{\alpha_i-1}c_i & p_i > b_i. \end{cases} \tag{16}$$

Evidently, $p_i = \frac{1}{3}[c_i + \sqrt{c_i^2 + \frac{3(\alpha_i+2)}{\alpha_i}b_i^2}]$ is the maximum when $b_i \ge \frac{\alpha_i}{\alpha_i-1}c_i$ while $p_i = \frac{\alpha_i}{\alpha_i-1}c_i$ is the maximum when $b_i < \frac{\alpha_i}{\alpha_i-1}c_i$. Note that when $b_i = \frac{\alpha_i}{\alpha_i-1}c_i$ then $\frac{1}{3}[c_i + \sqrt{c_i^2 + \frac{3(\alpha_i+2)}{\alpha_i}b_i^2}] = \frac{\alpha_i}{\alpha_i-1}c_i$.

For ease of illustration, we assume $\alpha_i = 10$ and $\delta_i = 2$. Then the maximization problem in (14) becomes:

$$\begin{aligned} &\max_{i\in\{1,2\}} \Pi_i(p_i) = \begin{cases} \lambda N[1-\frac{5}{6}(\frac{p_i}{b_i})^2](p_i-c_i) & c_i \le p_i \le b_i; \\ \frac{1}{6}\lambda N(\frac{b_i}{p_i})^{10}(p_i-c_i) & p_i > b_i, \end{cases} \\ &\text{subject to } U_1(p_{1_{opt}}) = U_2(p_{2_{opt}}) > 0, \\ &\text{and} \quad E_1(p_{1_{opt}}) + E_2(p_{2_{opt}}) \le 1. \end{aligned} \tag{17}$$

Thus, we obtain the optimal price as

$$p_{i_{opt}} = \begin{cases} \frac{1}{3}(c_i + \sqrt{c_i^2 + \frac{18}{5}b_i^2}) & c_i \le p_i \le b_i; \\ \frac{10}{9}c_i & p_i > b_i. \end{cases} \tag{18}$$

Clearly, for all $b_i \ge \frac{10}{9}c_i$, $p_i = \frac{1}{3}(c_i + \sqrt{c_i^2 + \frac{18}{5}b_i^2})$ is the maximum of the profit function defined in (17). Only when $b_i < \frac{10}{9}c_i$, $p_i = \frac{10}{9}c_i$ is the maximum. Since dynamic pricing is our main concern, in the rest of the paper we will only investigate the case of $b_i \ge \frac{10}{9}c_i$ and study the Nash equilibrium prices for this case.

Summarily, under the assumption $\alpha_i = 10$ and $\delta_i = 2$, solving the maximization problem shown in (17) for all $b_i \ge \frac{10}{9}c_i$ becomes solving the following maximization problem:

$$\begin{aligned} &\max_{i\in\{1,2\}} \Pi_i(p_i) = \lambda N[1-\frac{5}{6}(\frac{p_i}{b_i})^2](p_i-c_i) \quad p_i \ge c_i; \\ &\text{subject to } U_1(p_{1_{opt}}) = U_2(p_{2_{opt}}) > 0, \\ &\text{and} \quad E_1(p_{1_{opt}}) + E_2(p_{2_{opt}}) \le 1, \end{aligned} \tag{19}$$

where

$$E_i(p_i) = \begin{cases} 1-\frac{5}{6}(\frac{p_i}{b_i})^2; & c_i \le p_i \le b_i; \\ \frac{1}{6}(\frac{b_i}{p_i})^{10} & p_i > b_i, \end{cases}$$

Correspondingly, the optimal price is:

$$p_{i_{opt}} = \frac{1}{3}[c_i + \sqrt{c_i^2 + \frac{18}{5}b_i^2}] \tag{20}$$

In order to investigate Nash equilibrium in our model, we performed the following simulation in which two AP providers provide IP-based services in a WMN with $N = 30$ resale-users. Each resale-user generates packets according to a Poisson process with rate $\lambda = 10$packet/sec, and the service times of individual packet are i.i.d. exponentially distributed with mean $300^{-1}$sec. The costs of AP1 and AP2 per packet are $c_1 = 7$ and $c_2 = 5$ units respectively. We assume that both AP provider choose $\alpha = 10$ and $\delta = 2$. For $b_i \ge \frac{10}{9}c_i$, the optimal price, $p_{i_{opt}}$, is $\frac{1}{3}[c_i + \sqrt{c_i^2 + \frac{18}{5}b_i^2}]$.

Since a Nash equilibrium would exist when (2) holds, according to (5), the following expression can be derived:

$$p^*_{1_{opt}} - p^*_{2_{opt}} = \frac{5}{54}\lambda N[(\xi_1 + \sqrt{\xi_1^2 + \frac{18}{5}})^2 - (\xi_2 + \sqrt{\xi_2^2 + \frac{18}{5}})^2], \tag{21}$$

where $\xi_1 = \frac{c_1}{b_1}$ and $\xi_2 = \frac{c_2}{b_2}$. Combining the constraint condition $\sum_{i=1}^{2} E_i(p_i) \le 1$ with (21), pairs of prices $(p^*_{1_{opt}}, p^*_{2_{opt}})$ in Nash equilibrium can be obtained. Evidently, pairs of Nash equilibrium prices $(p^*_{1_{opt}}, p^*_{2_{opt}})$ are dependent on the ratio of the cost, $c_i$, and the parameter, $b_i$, of the probabilistic model for user's willingness-to-pay.

Table 1 lists some pairs of prices in Nash equilibrium, $(p^*_{1_{opt}}, p^*_{2_{opt}})$, and corresponding acceptance rates, $(E_1(p^*_{1_{opt}}), E_2(p^*_{2_{opt}}))$. As is observed, both APs have to set their price within a certain range so that $E_1(p^*_{1_{opt}}) + E_2(p^*_{2_{opt}}) \le 1$, Nash equilibrium can be reached. It implies that these two AP providers cannot increase their price as high as they want without cooperation. As shown in Table 1, when the AP2 with lower price increases its price higher than twice its cost, $E_2(p^*_{2_{opt}}) > 0.5$. As a response, AP1 with higher price also increases its price, which in turn lead to $E_1(p^*_{1_{opt}}) + E_2(p^*_{2_{opt}}) > 1$. For the sake of ease of simulation, AP$i$'s prices range from $c_i$ to $2c_i$ in our simulation.

In our simulation, $b_i$ is variable and $p_{i_{opt}}$ is calculated using (20). The pair of prices $(p^*_{1_{opt}},\ p^*_{2_{opt}})$ that can satisfy the constraint conditions in (19) are in Nash equilibrium. Note that $b_1$ and $b_2$ are variables. Thus, an unique pair of prices $(p^*_{1_{opt}},\ p^*_{2_{opt}})$ in Nash equilibrium could be obtained for each potential pair of $(b_1,\ b_2)$. Since $c_i \le p_i \le 2c_i$, $\frac{10}{9}c_i \le b_i \le \sqrt{\frac{20}{3}}c_i$ in our simulation.

Table 2 lists the resale-user's compensated utilities with the two APs under different prices. As can be observed, for example, if AP1 initially sets its price at 12.906 while AP2 initially sets its price at 5.635, $U_1(p_{1_{opt}}) < U_2(p_{2_{opt}})$ and the resale-users will choose to subscribe or switch

| | | | | | | |
|---|---|---|---|---|---|---|
| $p_1$ | 9.8033 | 10.77 | 11.71 | 12.78 | 13.28 | 13.688 |
| $b_1$ | 11.22 | 12.82 | 14.36 | 16.1 | 16.91 | 17.57 |
| $E_1$ | 0.3638 | 0.4118 | 0.4458 | 0.4749 | 0.4861 | 0.4942 |
| $p_2$ | 7.114 | 7.8227 | 8.6116 | 9.4802 | 9.9847 | 10.236 |
| $b_2$ | 8.2 | 9.44 | 10.66 | 12.07 | 12.74 | 13.29 |
| $E_2$ | 0.3727 | 0.4192 | 0.4562 | 0.4859 | 0.4973 | 0.5057 |

Table 1: Price versus acceptance Rate

to AP2. Then AP1 will have to decrease its price to attract more resale-users, while AP2 would increase its price considering its congestion situation or just leave its price unchanged. This price adjusting process will be repeated until $p_1$ and $p_2$ converge to the point at which the compensated utility experienced by the resale-users with AP1, $U_1$, is equal to the compensated utility experienced by the resale-users with AP2, $U_2$. For instance, AP1 decreases its price to 11.084 while AP2 increases its price to 8.112. At the point $U_1(p^*_{1_{opt}}) = U_{2_{opt}}(p^*_{2_{opt}})$, no AP has any incentive to deviate from its price without the cooperation of the other, which may not happen, until existing resale-users voluntarily disconnect or new resale-users join in.

When the number of resale-users in this market $N$ changes, $U_1(p_{1_{opt}})$ and $U_2(p_{2_{opt}})$ change, which in turn leads to the Nash equilibrium moving. This results in another round of seeking equilibrium among these two AP providers and the resale-users. As shown in Table 3, if we suppose in the first round the number of users $N = 30$ and the two APs end up with a Nash equilibrium with prices $p_1 = 11.818$ and $p_2 = 8.6976$ respectively. When the number of resale-users $N$ increases or decreases, even if AP1 keeps its price $p_1 = 11.818$, AP2 has to change its price such that both APs and the resale-users can reach a new equilibrium. Additionally, when some resale-users with one AP provider disconnect or some new resale-users join in one AP provider, the AP provider could adjust its price considering its resource utility or congestion situation. This also could lead to a new round of equilibrium seeking.

## 6. FUNCTIONAL VALIDATION

To verify the pricing model described in Section 5., we conduct simulations in which artificial traffic is generated to simulate resale-user behavior so that we can find the Nash equilibrium situation under which the resale-users' expected compensated utilities with both APs are equal and the corresponding Nash equilibrium prices for the two AP providers can be identified.

Simulations are performed on a hypothetical WMN with two APs who have Internet connectivity with identical available bandwidth 500kbps, and every resale-user can connect to both APs via a possible routing path. For the sake of clarity, we do our simulation with a simplified model in which all resale-users generate a random number of packets for a simple file transfer application in their session. Without loss of generality and so as to simplify the simulation, we assume that packets generated by the file transfer application are exponentially distributed with mean of 5000 bits. The time to transmit a packet with 5000 bits using the bandwidth 500kbps is 0.01sec. Thus, the service time of individual packet is exponentially distributed with a mean of 0.01sec.

The mechanism used to identify the resale-users' Nash equilibrium situation is described as follows.

**Resale-user Behavior for Quoted Prices**: Assume there are 15 resale-users in this WMN and each of them generates packets according to a Poisson process with mean rate of 10 packets/sec. Thus, the packets generated by these resale-users arrive according to a Poisson Process with mean rate of 150 packets/s to join the waiting queue of either of the two competing APs who serves its arriving packets using the FIFS scheduling scheme or opt out of both APs.

Every packet is associated with a random valuation which is generated based on the utility function presented in Section 4.. This random valuation determines whether the quoted price of one AP would be accepted and the packet would be sent.

Firstly, if the price quoted by the AP with higher price is greater than its valuation, the arriving packet, $j$, will not be sent to this AP and then we move to the AP with lower quoted price to conduct the same examination. Otherwise the arriving packet, $j$, would be submitted to the AP$i$ ($i = 1$ *or* $2$) with higher quoted price with a probability, $E_i$, determined by (4). If the arriving packet, $j$, cannot accept the prices quoted by both APs, it rejects the service and opts out of both APs.

In addition to the acceptability of the quoted price, for the arriving packet, $j$, the decision of which AP is submitted also depends on the load status of the potentially chosen AP, which is judged by the response time or mean packet delay (waiting time in the queue plus the service time), $s^i_j$, of the potentially chosen AP$i$'s ($i = 1$ *or* $2$) waiting queue at the time of its arrival. Thus, after it is certain that AP$i$'s quoted price is accepted, the expected gross utility with AP$i$, a function of the expected response time, $s^i_j$, needs to be examined. For instance, for the arriving packet, $j$, AP1's quoted price is accepted and the expected response time with the AP1 is $s^1_j$. The expected gross utility for the arriving packet, $V(s^1_j)$, is defined as $V(s^1_j) = 1/s^1_j$. Then if the expected compensated utility with AP1, the expected gross utility minus the corresponding quoted price, $1/s^1_j - p_1$, is positive, the arriving packet, $j$, enters AP1's waiting queue. If the expected compensated utility with AP1, $1/s^1_j - p_1$, is negative or zero, the arriving packet, $j$, chooses to bypass service on AP1.

**Pricing Policies**: Each AP provider AP$i$ computes its price that maximizes its own profit using the pricing scheme presented in Section 4.. Both AP providers choose $\alpha = 10$ and $\delta = 2$. Let AP1's price strategy form be $\{p^1_1, p^2_1, \cdots, p^n_1\}$ and AP2's price strategy form be $\{p^1_2, p^2_2, \cdots, p^n_2\}$.

| | | | | | | | | |
|---|---|---|---|---|---|---|---|---|
| $p_1$ | 8.246 | 8.995 | 9.791 | 10.237 | 11.084 | 11.818 | 12.478 | 12.906 | 13.685 |
| $U_1$ | 222.13 | 198.83 | 181.27 | 173.54 | 161.64 | 153.44 | 147.26 | 143.73 | 138.06 |
| $p_2$ | 5.635 | 6.602 | 7.552 | 7.774 | 8.112 | 8.474 | 9.187 | 9.452 | 10 |
| $U_2$ | 239.16 | 195.38 | 171.46 | 167.29 | 161.64 | 156.37 | 147.75 | 145.02 | 140 |

Table 2: resale-users' Compensated Utilities

| | | | | | | | | | | |
|---|---|---|---|---|---|---|---|---|---|---|
| $N=5$ | $p_1$ | 8.246 | 8.9975 | 9.7912 | 10.237 | 11.084 | 11.818 | 12.112 | — | — |
| | $U_1$ | 280.15 | 275.64 | 272.05 | 270.39 | 267.7 | 265.73 | 265 | — | — |
| | $\Pi_1$ | 14.46 | 30.64 | 50.68 | 62.71 | 86.63 | 108.19 | 117 | — | — |
| | $p_2$ | 6.1613 | 6.8438 | 7.6099 | 8.0513 | 8.9159 | 9.6874 | 10 | — | — |
| | $U_2$ | 280.15 | 275.65 | 272.05 | 270.39 | 267.7 | 265.72 | 265 | — | — |
| | $\Pi_2$ | 15.90 | 32.28 | 53.09 | 65.78 | 91.56 | 115.26 | 125 | — | — |
| $N=10$ | $p_1$ | 8.246 | 8.9945 | 9.7912 | 10.237 | 11.084 | 11.818 | 12.478 | 12.7 | — |
| | $U_1$ | 268.55 | 260.28 | 253.9 | 251.02 | 246.49 | 243.27 | 240.77 | 240 | — |
| | $\Pi_1$ | 28.92 | 61.28 | 101.36 | 125.41 | 173.27 | 216.37 | 256.11 | 269.61 | — |
| | $p_2$ | 6.0265 | 6.6407 | 7.3191 | 7.7071 | 8.4705 | 9.1531 | 9.7964 | 10 | — |
| | $U_2$ | 268.56 | 260.29 | 253.89 | 251.03 | 246.49 | 243.27 | 240.77 | 240 | — |
| | $\Pi_2$ | 26.09 | 54.26 | 89.96 | 111.7 | 156.3 | 197.58 | 236.68 | 250 | — |
| $N=20$ | $p_1$ | 8.246 | 8.9945 | 9.7912 | 10.237 | 11.084 | 11.821 | 12.481 | 12.906 | 13.187 |
| | $U_1$ | 245.34 | 229.56 | 217.59 | 212.28 | 204.06 | 198.33 | 194 | 191.52 | 189.99 |
| | $\Pi_1$ | 57.83 | 122.56 | 202.71 | 250.82 | 346.54 | 433.11 | 512.59 | 584.49 | 599.03 |
| | $p_2$ | 5.9594 | 6.5336 | 7.1592 | 7.5159 | 8.2071 | 8.8205 | 9.3845 | 9.7544 | 10 |
| | $U_2$ | 245.33 | 229.57 | 217.59 | 212.28 | 204.05 | 198.34 | 194.01 | 191.5 | 190 |
| | $\Pi_2$ | 47.74 | 97.99 | 162.48 | 201.78 | 281.39 | 354.68 | 423.58 | 469.5 | 500 |
| $N=30$ | $p_1$ | 8.246 | 8.9945 | 9.7912 | 10.237 | 11.084 | 11.818 | 12.478 | 12.906 | 13.685 |
| | $U_1$ | 222.13 | 198.83 | 181.24 | 173.54 | 161.64 | 153.44 | 147.26 | 143.73 | 138.06 |
| | $\Pi_1$ | 86.75 | 183.84 | 304.07 | 376.23 | 519.8 | 649.12 | 768.32 | 846.73 | 991.04 |
| | $p_2$ | 5.9361 | 6.498 | 7.105 | 7.4492 | 8.1124 | 8.6976 | 9.2333 | 9.5853 | 10.236 |
| | $U_2$ | 222.13 | 198.83 | 181.27 | 173.54 | 161.64 | 153.44 | 147.26 | 143.73 | 138.06 |
| | $\Pi_2$ | 67.34 | 141.81 | 234.96 | 291.49 | 405.39 | 509.75 | 607.48 | 672.59 | 794.28 |
| $N=35$ | $p_1$ | 8.246 | 8.9975 | 9.7912 | 10.237 | 11.084 | 11.821 | 12.478 | 12.906 | 13.474 |
| | $U_1$ | 210.53 | 183.38 | 163.12 | 154.17 | 140.42 | 130.95 | 123.89 | 119.84 | 115 |
| | $\Pi_1$ | 101.21 | 214.97 | 354.74 | 438.94 | 606.44 | 757.95 | 896.38 | 987.85 | 1110.5 |
| | $p_2$ | 5.9303 | 6.4891 | 7.09 | 7.431 | 8.8049 | 8.6638 | 9.1901 | 9.5358 | 10 |
| | $U_2$ | 210.48 | 183.41 | 161.1 | 154.14 | 140.43 | 130.96 | 123.88 | 119.83 | 115 |
| | $\Pi_2$ | 77.76 | 163.91 | 271.3 | 336.53 | 467.33 | 587.59 | 699.46 | 773.97 | 875 |
| $N=40$ | $p_1$ | 8.246 | 8.9975 | 9.7912 | 10.237 | 11.084 | 11.818 | 12.478 | 12.909 | 13.53 |
| | $U_1$ | 198.92 | 168.11 | 144.96 | 134.8 | 119.21 | 108.53 | 100.51 | 95.91 | 90 |
| | $\Pi_1$ | 115.67 | 245.12 | 405.42 | 501.64 | 693.07 | 865.5 | 1024.4 | 1129.7 | 1282.9 |
| | $p_2$ | 5.9245 | 6.4801 | 7.0779 | 7.4159 | 8.0635 | 8.6362 | 9.1562 | 9.4988 | 10 |
| | $U_2$ | 198.93 | 168.09 | 144.95 | 134.78 | 119.23 | 108.51 | 100.51 | 95.92 | 90 |
| | $\Pi_2$ | 87.96 | 185.66 | 307.48 | 381.24 | 529.1 | 664.89 | 791.08 | 875.37 | 1000 |
| $N=50$ | $p_1$ | 8.246 | 8.9945 | 9.7912 | 10.237 | 11.084 | 11.818 | 12.481 | 12.906 | 13.614 |
| | $U_1$ | 175.72 | 137.39 | 108.65 | 96.06 | 76.78 | 63.62 | 53.72 | 48.16 | 39.99 |
| | $\Pi_1$ | 144.58 | 306.4 | 506.78 | 627.06 | 806.34 | 1081.9 | 1281.5 | 1411.2 | 1629.6 |
| | $p_2$ | 5.9187 | 6.4683 | 7.0599 | 7.3947 | 8.0361 | 8.5962 | 9.1099 | 9.4432 | 10 |
| | $U_2$ | 175.64 | 137.41 | 108.69 | 96.06 | 76.77 | 63.63 | 53.73 | 48.15 | 40 |
| | $\Pi_2$ | 209.95 | 288.67 | 517.49 | 629.44 | 707.32 | 842.3 | 935.83 | 1087.6 | 1181.6 |

Table 3: Users' Compensated Utilities for Different Number of Users $N$

We start by finding equilibrium for the resale-users, given that AP1 charges $p_1^1$ and AP2 charges $p_2^1$. We proceed by keeping the price charged by AP1 fixed at $p_1^1$, while the price charged by AP2 continuously changes according to its price strategy form $\{p_2^1, p_2^2, \cdots, p_2^n\}$. The continuous price change leads to a corresponding continuous change to the expected compensated utilities of the resale-users. This allows us to identify the expected compensated utilities of the resale-users for any pair of prices $(p_1^n, p_2^n)$. In particular, the equilibrium compensated utilities that correspond to the pairs of Equilibrium prices, $(p_1^*, p_2^*)$, are identified.

Fig. 6 compares the simulation $U_2 - U_1$ with the analytical one. As can be observed, the surface of the figure reflecting the simulation result in Fig. 6 (a) contains significant numerical noise. Fig. 7 plots the equilibrium prices of simulation and analysis respectively. As can be seen, even though the curve of the simulation equilibrium prices are not as smooth as the analytical one, the tendency of the simulation curve approaches the smooth curve of the analytical equilibrium prices.

Fig. 8 and Fig. 9 compare the analytical equilibrium prices with the simulation equilibrium prices under N=10 and 20 respectively. As can be observed, among Fig. 7, Fig. 8 and Fig. 9, while the tendency of all the simulation equilibrium prices curve are close to their corresponding analytical ones, the simulation equilibrium prices curve under N = 15 (in Fig. 7) coincides with the corresponding analytical one most closely.

Under N=10, the gradients of the simulation equilibrium curves coincide with the corresponding analytical ones in the higher-price area. These indicate that the similarity between the simulation equilibrium curve and the analytical one depends on the traffic intensities, $\rho_i = \frac{\lambda N E_i(p_i)}{\mu}$, of both APs. As mentioned in Section 5. that theoretically $0.26 < E_i(p_{i_{opt}}^*) \leq 0.5$ when $\frac{10}{9}c_i \leq b_i \leq \sqrt{\frac{20}{3}}c_i$, accordingly when $N = 10$, $0.26 < \rho_i \leq 0.5$, which illustrates that the utilization of both APs are at an inefficient level when their prices are lower. Under $N = 20$, the gradients of the simulation equilibrium curves coincide with the corresponding analytical ones in the lower-price area, for instance $\{[7.7, 9.8], [5.5, 7.2]\}$, where $0.35 < \rho_i < 0.7$ (estimated value).

Summarily, Fig. 7, 8 and 9 imply that when the traffic intensity of each AP satisfies $0.35 < \rho_i < 0.80$ (estimated value) the gradients of the simulation curves coincide with those of the analytical results. In other words, the simulation results coincide with the analytical results when the utilization of both APs are at a stable and efficient level.

According to (5), theoretically when $N = 25$ the expected compensated utility $U_i(p_i) \leq 0$ if the expected acceptance rate $E_i(p_i) \geq \frac{100 - p_i}{250}$. It is mainly because $\rho_i = \frac{\lambda N E_i(p_i)}{\mu} \geq 1$ when $E_i(p_i) \geq 0.4$, which means that the packets arrive faster than they are served and the delay is much longer than that of a stable system. In other words, the queue of the AP will grow to an infinite length, thus the expected number of jobs in the system cannot be defined. Therefore, theoretically the equilibrium prices $(p_{1_{opt}}^*, p_{2_{opt}}^*)$ must fall into the range of $\{[7.7334, 10.455], [5.5238, 7.4765]\}$ respectively when $N = 25$. Thus, 10.455 and 7.4765 can be called critical prices for AP1 and AP2 respectively when $N = 25$.

However, even though statistically when $\rho_i = \frac{\lambda N E_i(p_i)}{\mu} \geq 1$ (mean packet delay $ED_i = \mu - \lambda N E_i(p_i) \leq 0$) it is impossible to analyze the service system of the AP mathematically, simulation results, shown in Fig. 10(a) and (b), show that the simulation equilibrium prices are close to the analytical ones within the range of $\{[7.7334, 10.455], [5.5238, 7.4765]\}$, and equilibration still can be reached even for the prices out of the range of $\{[7.7334, 10.455], [5.5238, 7.4765]\}$. The explanation could be that some packets give up service because of the long delay so that some other packets have a chance to be served with a shorter than expected delay, which can satisfy their compensated utility. The compensated utilities of those packets entering the waiting queue of the two AP respectively then reach equilibrium and the equilibrium prices can then be identified. As is observed, for a given $p_1$ which is greater than 10.455, which leads to the queue system of AP1 being unstable, the corresponding equilibrium price $p_2$ is around 7.4765, which is the critical price for AP2. In other words, even though AP1 sets a price $p_1$ that results in unstable queue system, the packets that have a chance to enter into the waiting queue of AP1 still reach an equilibrium with the packets that join AP2 when AP2 sets a critical price such that its queue system remains stable.

Similarly, when $N = 30$, the analytical equilibrium prices $(p_{1_{opt}}^*, p_{2_{opt}}^*)$ should fall into the range of $\{[7.7334, 9.3125], [5.5238, 6.6347]\}$ respectively. Simulation results, shown in Fig. 10(c) and (d), show that equilibration can be reached even if both APs choose their prices out of the range of $\{[7.7334, 9.3125], [5.5238, 6.6347]\}$. Note that the slope of the simulation equilibrium curve under $N = 30$ in Fig. 10(d) is lower than that of the simulation equilibrium curve under $N = 25$ in Fig. 10(b). The reason is that theoretically under $N = 30$ AP2's critical price is lower than that of the case of $N = 25$.

Simulation results for $N = 40$ are illustrated in Fig. 10(e) and (f). As can be observed, when $N = 40$, under which the expected compensated utilities with both APs, $\mu - \lambda N E_i(p_i) - p_i < 0$ $(i = 1, 2)$, for all potential prices theoretically, equilibria still exist. However, the simulation equilibrium price distribution is random as shown in in Fig. 10(f). It could be explained as following: when $N = 40$, given any potential prices, $\rho_i = \frac{\lambda N E_i(p_i)}{\mu} \geq 1$ $(i = 1, 2)$ and the service system of both AP are unstable, which leads to the packets that join both APs with a shorter time delay being distributed randomly.

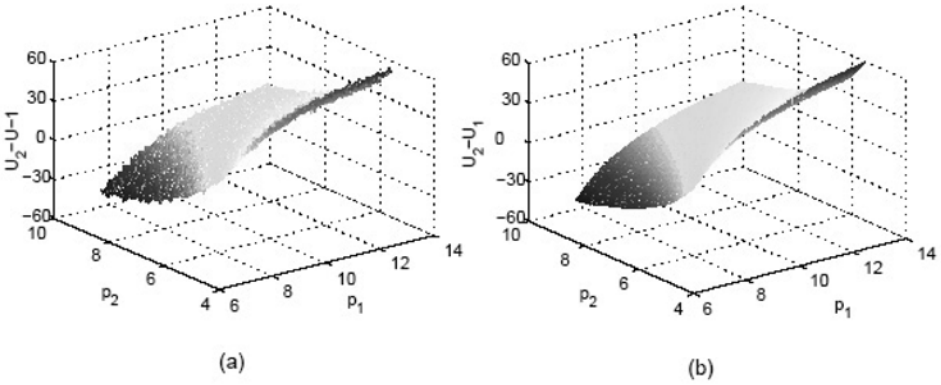


Fig 6: Simulation- versus Analytical Equilibrium (the number of resale-users N = 15): (a) Simulation value difference between U2(p2) and U1(p1), U2(p2)−U1(p1); (b) Analytical value difference between U2(p2) and U1(p1), U2(p2)−U1(p1).

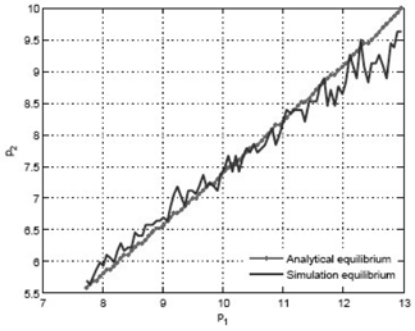


Fig7: Simulation- versus Analytical Equilibrium (the number of resale-users N = 15): Equilibrium prices corresponding to simulation and analysis respectively.

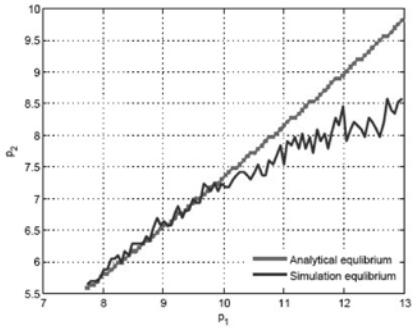


Fig 9: Simulation- versus Analytical Equilibrium (the number of resale-users N = 20): Equilibrium prices corresponding to simulation and analysis respectively

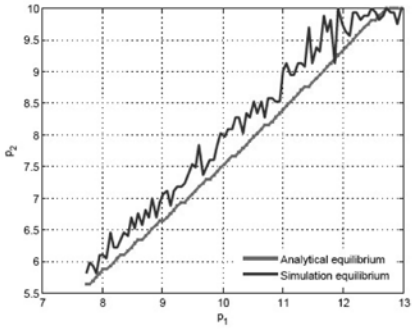


Fig 8: Simulation- versus Analytical Equilibrium (the number of resale-users N = 10): Equilibrium prices corresponding to simulation and analysis respectively.

## 7. CONCLUSIONS

This paper has developed an analysis framework of a pricing scheme for WMNs under two competing AP providers and congestion-sensitive resale-users, and introduced a mathematical pricing model. With this pricing method, resale-user's expected compensated utility, which is a function of the prices and QoS offered by APs, is the key factor for the two APs to determine their prices such that a Nash equilibrium can be achieved. A numerical example is provided to show the existence and uniqueness of Nash equilibrium. The introduction of the parameterized customer behavior model proposed by Jagannathan *et al*. [6] allows this pricing method to be able to capture the change of the end-user's compensated utility. Therefore, when the market situation changes, which in turn could result in a change in the existing equilibrium, the AP providers can adjust their prices based on the end-user's newly compensated utility to reach a new equilibrium. The numerical example has shown how the two AP providers with differing costs set their prices so that Nash equilibrium can be reached. Sensitivity analysis shows that the equilibrium prices are sensitive to demand scenarios. Simulations are conducted to validate the analytical results.

## REFERENCES

[1] S. K. Das, M. Chatterjee, and H. Lin, "An econometric model for resource management in competitive wireless data networks," *IEEE Network*, pp. 20–26, November/December 2004.

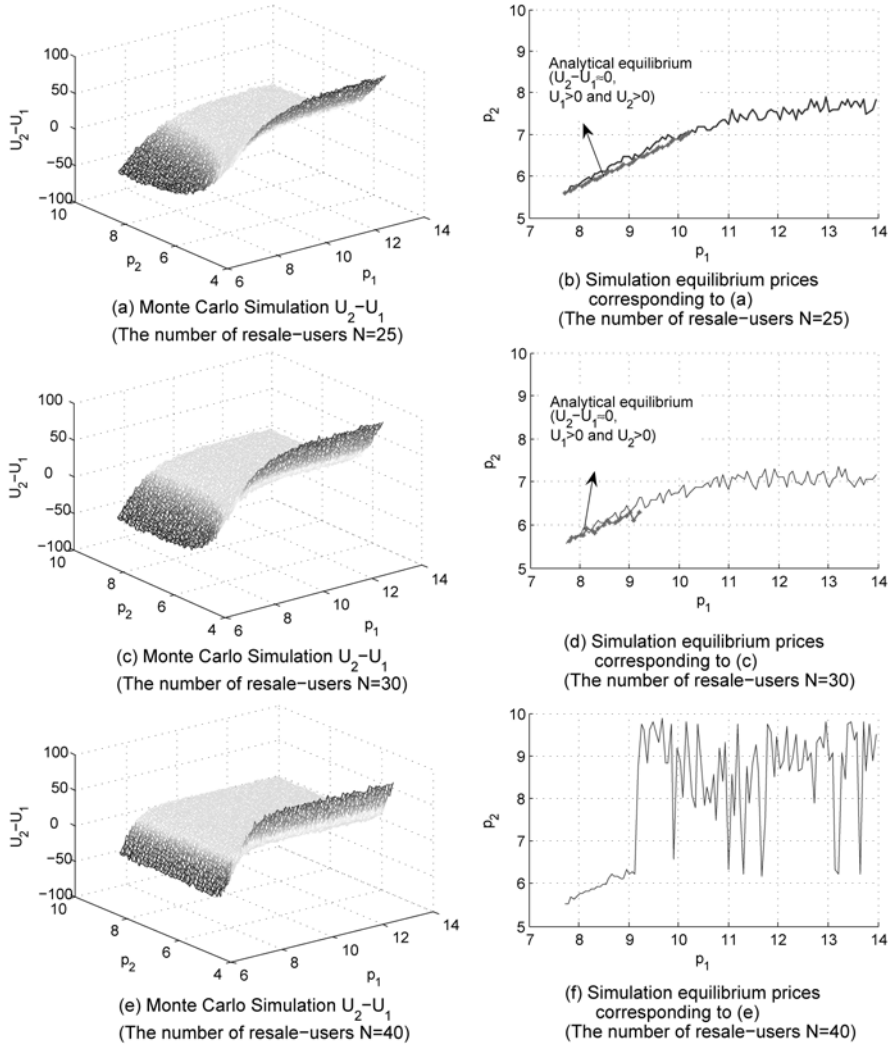


Fig 10: Simulation Equilibria. (a) Simulation value difference between U2(p2) and U1(p1), U2(p2)−U1(p1), when the number of resale-users N = 25; (b) Equilibrium prices when the number of resale-users N = 25;(c) Simulation value difference between U2(p2) and U1(p1), U2(p2)−U1(p1), when the number of resale-users N = 30; (d) Equilibrium prices when the number of resale-users N = 30; (e) Simulation value difference between U2(p2) and U1(p1), U2(p2)−U1(p1), when the number of resale-users N = 40; (f) Equilibrium prices when the number of resale-users N = 40.

[2] M. L. Best and C. M. Maclay, "Community internet access in rural areas: Solving the economic sustainability puzzle," 2002. [Online]. Available: http://www.cid.harvard.edu/cr/pdf/gitrr2002_ch08.pdf

[3] R. Gibbens, R. Mason, and R. Steinberg, "Internet service classes under competition," *IEEE Journal on Selected Areas in Communications*, vol. 18, no. 7, pp. 2490–2498, 2000.

[4] H. Mendelson, "Pricing computer services: Queuing effects," *Communications of the ACM*, vol. 28, no. 3, pp. 312–321, 1985.

[5] N. C. Hock, *Queuing Modeling Fundamentals*. John Wiley and Sons Ltd, 1996.

[6] S. Jagannatha, J. Nayak, K. Almeroth, and M. Hofmann, "A model for discovering customer value for e-content," *ACM SIGKDD*, July 2003.